LONG-TAILED REPRESENTATION LEARNING VIA FEATURE SPACE RECONSTRUCTION

Anonymous authors
Paper under double-blind review

ABSTRACT

Deep learning has achieved significant success on balanced datasets. However, real-world data often exhibit a long-tailed distribution. Empirical results show that long-tailed data skews representations where head classes dominate the feature space. Many methods have been proposed to empirically correct the skewed representations. However, a clear theoretical understanding of the underlying causes and extent of this skew remains lacking. In this work, we provide a comprehensive theoretical analysis to elucidate how long-tailed data affects representations, deriving the conditions under which the centers of the tail classes shrink together or even collapse into a single point. This results in overlapping feature distributions of tail classes, making features in the overlapping regions inseparable. Moreover, we demonstrate that merely empirically correcting the skewed representations of training data is insufficient to separate the overlapping features, due to distribution shifts between training and real data. To address these challenges, we propose a novel long-tailed representation learning method, FeatRecon. It reconstructs the feature space so that features of all classes are arranged into symmetrical and linearly separable regions. Thereby, it enhances model robustness to long-tailed data. We validate the effectiveness of our method through extensive experiments on the CIFAR-10-LT, CIFAR-100-LT, ImageNet-LT, and iNaturalist 2018 datasets.

1 INTRODUCTION

Deep learning has achieved significant success on balanced datasets (Deng et al., 2009). However, in real-world scenarios, collected datasets often exhibit long-tailed distributions. *Class distribution*, i.e., the sample sizes of different classes, is highly imbalanced. Many classes contain only a few samples (called *tail classes*), whereas a few classes have a large number of samples (called *head classes*). Training on such datasets distorts a model's feature representations and decision boundaries, and thus limits the model's generalization capability and performance on test data.

Our understanding of balanced data representation has advanced significantly. For instance, using the powerful representation learning tool, *contrastive learning* (Khosla et al., 2020), it has been shown (Graf et al., 2021) that for balanced data, when the *supervised contrastive loss* (SC loss) reaches its minimum, the representations of each class converge at their respective class centers, and all class centers form a regular simplex (see Theorem 1 and Fig. 1a). This highly symmetrical configuration ensures separation between different classes, resulting in strong classification performance. However, for imbalanced data, the optimal representation configuration remains poorly understood.

When data follows a long-tailed distribution, empirical studies suggest that the optimal representations form an asymmetrical configuration, with head classes dominating the feature space. While several methods (Zhu et al., 2022; Kang et al., 2021; Li et al., 2022; Du et al., 2024) have attempted to correct this asymmetry, they primarily rely on empirical adjustments. Crucially, none of these methods provide a theoretical explanation of why and to what extent head classes dominate the feature space. Understanding this could offer deeper insights into learning better representations of long-tailed data, and inspire novel methods.

In this paper, we study long-tailed data representation and establish the first theoretical framework (in Theorem 2) for the optimal representation configuration, i.e., the arrangement of class centers when the SC loss is minimized, under various class distributions. In particular, we derive the analytical relationship between the imbalance factor, i.e., the ratio of sample sizes between head and tail classes,

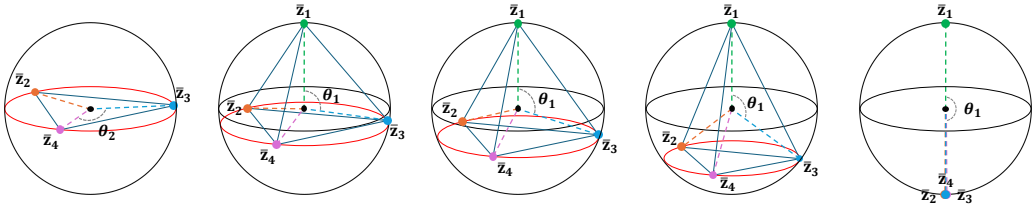

(a) $\rho = 0$ (b) $0 < \rho < 1$ (c) $\rho = 1$ (d) $1 < \rho < R$ (e) $\rho \geq R$

Figure 1: The optimal representation configuration for four classes with different imbalance factors, ρ. Centers of the four classes ($\bar{z}_1, \ldots, \bar{z}_4$) are positioned on a unit hypersphere. Assume classes 2, 3 and 4 have the same size, $N_2 = N_3 = N_4$. Class 1's size is their size multiplied by ρ, $N_1 = \rho N_2$. **(a)**: when class 1 is empty ($N_1 = 0$), classes 2, 3 and 4 form a regular simplex. **(b) to (e)**: As ρ increases and N_1 increases, $\bar{z}_2$, $\bar{z}_3$ and $\bar{z}_4$ are pushed away from the equator and eventually collapse. **(c)**: when $\rho = 1$, all four classes form a regular simplex. R is the critical constant at which the collapse happens (see Sec. 3 for details). θ_1 is the angle between the head class center and tail class centers, and θ_2 is the angle between tail classes.

and the angles between different class centers at the optimal configuration. We show that as the imbalance factor increases, the head class increasingly dominates the feature space, pushing the centers of the tail classes closer together . Beyond a certain critical threshold, the centers of the tail classes collapse into a single point. Fig. 1 illustrates the optimal configuration of four classes. From Fig. 1a to Fig. 1e, as the imbalance factor continuously increases, the center of the head class ($\bar{z}_1$) pushes the other three tail classes' centers ($\bar{z}_2$, $\bar{z}_3$ and $\bar{z}_4$) closer and eventually collapse (Fig. 1e).[1]

Our theory provides insights into how long-tailed data hurts the representation learning. Without any mitigation strategy, tail classes are pushed close to one another or even collapse, resulting in overlapping distributions and poor separability between them. To address this issue, existing methods often readjust the empirical tail class centers to a symmetric configuration. However, due to the limited sample sizes of tail classes, these approaches may over-correct the issue, forcing the true centers of the tail classes to be too close to the head class, leading to overlapping distributions and poor separability between head and tail classes.

In this paper, we introduce **FeatRecon**, a novel method for long-tailed representation learning. It reconstructs the feature space so that features of all classes are arranged into symmetrical and linearly separable regions. Inspired by the theoretical analysis, our method addresses the center skewing issue by rebalancing the sample sizes of all classes. This is achieved by generating synthetic features for tail classes and using both real and synthetic features for representation learning. To ensure that features of different classes are linearly separable, the synthetic features of one class are constrained within an estimated *confidence support*, i.e., the feature space region covering the majority of samples in a class. We derive the necessary condition for the confidence supports to ensure they do not overlap at the optimal configuration.

The estimation of confidence support is crucial to our method. Direct estimation of the feature distribution is challenging due to the non-Euclidean geometry of the normalized feature space and the limited sample size of tail classes. Instead, we estimate the confidence support simply using the center of each class and a single "central angle" parameter. Since the tail class estimation can be unreliable, the statistics of tail classes are regularized using the statistics of head classes. By iteratively generating synthetic features to fill these confidence supports, adjusting representations, and re-estimating confidence supports, we can learn a feature space in which both head and tail classes are equally separated, with no overlap between their confidence supports.

Our contributions are summarized as follows:

- We provide a theoretical analysis of how long-tailed data skews the feature representation and how the skewed representation limits the model's generalization capability.

[1]For completeness, our analysis encompasses the cases when class 1's size, N_1, is smaller than the others'. Technically, class 1 is not the head class any more when $N_1 \leq N_2 = N_3 = N_3$.

- We propose a novel algorithm to generate synthetic features to balance the sample sizes of all classes. And synthetic features are constrained within confidence supports which are estimated with regularization of statistics of head classes.
- We propose an iterative approach to learn a symmetric and linearly separable feature space for long-tailed data. Our method iteratively generating synthetic features, adjusting representations, and re-estimating confidence support.

We validate our method with thorough experiments on four commonly-used datasets. Our method outperforms SOTA performance compared to widely adopted long-tailed learning baselines.

2 Related Work

2.1 Long-tailed Recognition

Resampling (Byrd & Lipton, 2019) and *re-weighting* (Cui et al., 2019; Jamal et al., 2020; Chen et al., 2023) are two classical methods in long-tailed learning. The former balances the number of training samples among different classes by either oversampling the tail classes or downsampling the head classes. The latter balances the per-class contributions to the loss function by assigning higher weights to classes with smaller gradients. Other methods adjust decision boundaries through either *post-hoc weight normalization* (Dang et al., 2024) or *margin adjustment* (Cao et al., 2019; Menon et al., 2021; Khan et al., 2019). The former balances the decision boundaries by adjusting the weight norms of classifiers, while the latter increases the margins of the tail classes. Recent works also explore ideas in *data augmentation* (Ahn et al., 2023; Gao et al., 2024), which adjusts the strength of class-wise augmentation to help learn class-balanced representations, and *transfer learning* (Chen & Su, 2023; Zhang et al., 2023), which leverages information from the head classes to improve learning of the tail classes. A common way for transfer learning is to assume that data follows a multivariate Gaussian distribution and transfer distribution statistics. However, robust parameters estimation (i.e., the $K \times K$ covariance matrix) can be challenging given the small sample sizes of tail classes, and the distributional assumption does not hold for normalized features.

2.2 Contrastive Learning for Long-tailed Data

Contrastive learning (He et al., 2020; Chen et al., 2020; Caron et al., 2020; Chen & He, 2021; Grill et al., 2020; Wang & Isola, 2020) has made tremendous progress as a representation learning tool. Supervised contrastive learning (SCL) (Khosla et al., 2020), by optimizing the supervised contrastive loss, learns a symmetrical feature space where the representations of each class collapse to the vertices of a regular simplex. (Graf et al., 2021).

Recent studies in *long-tailed learning* (LTL) (Wang et al., 2021; Cui et al., 2021; Xuan & Zhang, 2024) incorporate an SCL module into the LTL framework, aiming to learn better representations and improve classifier training. However, directly using SCL is not ideal, as some (Li et al., 2022; Zhu et al., 2022) have demonstrated that SCL skews the feature space when training on long-tailed data. Many methods then focus on empirically readjusting these skewed representations. TCL (Li et al., 2022) addresses this by predefining well-separated empirical centers. Other methods re-balance the number of contrastive pairs in the SC loss, i.e, positive pairs (Kang et al., 2021), negative pairs (Zhu et al., 2022), or both positive and negative pairs (Du et al., 2024). Our method balances both positive and negative pairs by generating new features for the tail classes in hyperspherical caps. It involves estimating only two parameters, with tail class statistics regularized using those of the head classes.

3 Theoretical Analysis: Long-tailed Data Skews Contrastive Feature Representation

In this section, we study how long-tailed data skews the feature space. To understand how varying class distributions influence representations, we provide a theoretical framework (in Sec. 3.2) to investigate the optimal representation configuration when the SC loss is minimized (see Fig. 1).

We show (in Theorem 1), for balanced data, the optimal representations form a regular simplex. This reveals that representations of different classes are equally separated to the largest extent.

However, for imbalanced data, the optimal representation configuration becomes far more complex. Therefore, we focus on a one-vs-all scenario. We adjust the sample size of class 1, while assuming the remaining $K-1$ classes have equal and fixed sample size. In Theorem 2, we study the geometry of the optimal representation configuration when the imbalance factor changes.

3.1 PRELIMINARIES

Suppose we have N training samples, $X = (x_1, \ldots, x_N) \in (\mathcal{X})^N$, randomly drawn from K distinct classes, with labels $Y = (y_1, \ldots, y_N) \in (\mathcal{Y})^N$ and $\mathcal{Y} = [K] = \{1, \ldots, K\}$. A unit hypersphere (in $\mathbb{R}^h$) is defined as $\mathbb{S}^{h-1} = \left\{z \in \mathbb{R}^h : \|z\| = 1\right\}$. An encoder is a map $\varphi : \mathcal{X} \to \mathbb{R}^h$ that extracts representations from data, denoted as $Z = (\varphi(x_1), \ldots \varphi(x_N))$.

In practice, contrastive learning is conducted batch-wise due to memory limitations. To simplify our analysis, we assume unlimited memory to train on all samples in a single batch. We denote the set of indices of all samples as $B = [N] = \{1, \ldots, N\}$, and the set of indices of samples from the class k as $B_k = \{i : i \in B, y_i = k\}$. Let N_k be the number of samples from class k, $N_k = |B_k|$ and $N = \sum_{k=1}^{K} N_k$. The following definitions are necessary for the study.

Definition 1 (Supervised contrastive loss (SC loss))**.** *Let Z be an N point configuration (assuming all z's being normalized), $Z = (z_1, \ldots, z_N) \in (\mathbb{S}^{h-1})^N$, with labels $Y = (y_1, \ldots, y_N) \in ([K])^N$, and $3 \leq K \leq h+1$. The supervised contrastive loss $\mathcal{L}_{\mathrm{SC}}(\cdot; Y) : (\mathbb{S}^{h-1})^N \to \mathbb{R}$ is defined as*

$$\mathcal{L}_{\mathrm{SC}} = \sum_{k=1}^{K} \sum_{i \in B_k} \mathcal{L}_{\mathrm{SC}}^{k,i}, \text{ where } \mathcal{L}_{\mathrm{SC}}^{k,i} = -\frac{\mathbb{1}_{\{N_k > 1\}}}{N_k - 1} \sum_{j \in B_k \setminus \{i\}} \log \left(\frac{\exp\left(\langle z_i, z_j \rangle / \tau\right)}{\sum_{l \in B \setminus \{i\}} \exp\left(\langle z_i, z_l \rangle / \tau\right)} \right) \quad (1)$$

Definition 2 (Equidistant/regular simplex)**.** *Let $h, K \in \mathbb{N}$ with $K \leq h+1$. An K point configuration $\zeta = (\zeta_1, \ldots, \zeta_K) \in (\mathbb{S}^{h-1})^N$ form the vertices of an equidistant simplex inscribed in the unit-hypersphere, if and only if the following conditions hold:*

(1) $\forall i \in [K], \|\zeta_i\| = 1$

(2) $\exists d \in \mathbb{R}, \forall i, j$ *and* $1 \leq i < j \leq K$, $d = \langle \zeta_i, \zeta_j \rangle$

And ζ form the vertices of a regular simplex inscribed in the unit-hypersphere, if and only if (1), (2) and the following condition holds:

(3) $\sum_{i \in [K]} \zeta_i = 0$

3.2 OPTIMAL REPRESENTATION CONFIGURATION

In this subsection, we assume a sufficiently powerful encoder capable of realizing any representation configuration, and set the temperature parameter (in Eq. (1)) to $\tau = 1$.

Optimal Representation Configuration for Balanced Data. When data is balanced, Theorem 1 states that the SC loss attains its minimum if and only if the representations of each class converge at their respective class centers, and the centers of all classes form a regular simplex.

Theorem 1. *Let Z be an N point configuration (assuming all zs being normalized), $Z = (z_1, \ldots, z_N) \in (\mathbb{S}^{h-1})^N$, with labels $Y = (y_1, \ldots, y_N) \in ([K])^N$, and $3 \leq K \leq h+1$. When Y is balanced, hence $\forall i \in [K]$, $N_k = \frac{N}{K}$, it holds that:*

$$\mathcal{L}_{\mathrm{SC}} \geq N \log \left(\left(\frac{N}{K} - 1 \right) + \frac{N(K-1)}{K} \exp\left(-\frac{K}{K-1} \right) \right) \quad (2)$$

where equality is attained if and only if there exists a configuration of $\bar{Z} = (\bar{z}_1, \ldots, \bar{z}_K) \in (\mathbb{S}^{h-1})^K$ such that:

(A1) $i \in B_k$, $z_i = \bar{z}_k$.

(A2) $\bar{Z}$ *form a regular simplex inscribed in the unit-hypersphere.*

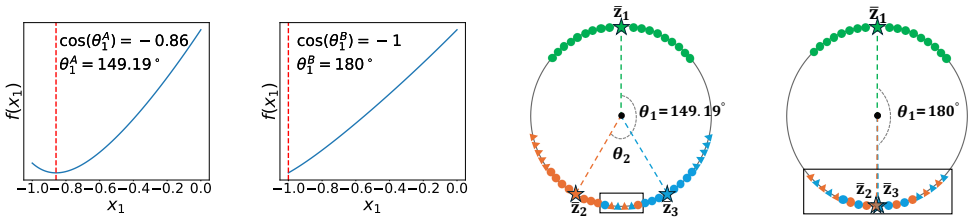

(a) (b) (c) (d)

Figure 2: Numerical example. The sample size ratio is **10:1:1** in Example A and **100:1:1** in Example B. (a) $f(x_1)$ of Example A. (b) $f(x_1)$ of Example B. (c) Representations of Example A. (d) Representations of Example B. Stars are empirical centers. Circles are available samples, triangles are missing samples. Black boxes are overlapping regions.

Remark 1. *This theorem has been previously established (Graf et al., 2021). In this paper, we provide a new proof (Appendix B.1) that dose not presume $\mathcal{L}_{\mathrm{SC}}^{k,i}$ (in Eq. (1)) to be the same when k varies, as was done in (S39) of (Graf et al., 2021). This allows us to extend the analysis to more general center configurations, particularly laying the foundation for the imbalanced data case (Theorem 2).*

Optimal Representation Configuration for Imbalanced Data. When data is imbalanced, we first find the tight lower bound function f of $\mathcal{L}_{\mathrm{SC}}$, assuming all representations converging at their respective class centers. f only depends on the center configuration. We then determine the optimal representation configuration when f is minimized. When there are one imbalanced class and $K-1$ balanced classes, Theorem 2 states the SC loss is minimized if and only if the representations of classes 2 to K converge to the vertices of an equidistant simplex while representations of class 1 converge to the point that is perpendicular to the equidistant simplex (more explanations in Appendix A.2)

Theorem 2. *Let Z be an N point configuration (assuming all zs being normalized), $Z = (z_1, \ldots, z_N) \in (\mathbb{S}^{h-1})^N$, with labels $Y = (y_1, \ldots, y_N) \in ([K])^N$, and $3 \leq K \leq h+1$. If $\forall k \in \{2, \ldots, K\}, N_k = a_2 \geq 4$, and $\exists \rho > 0$ such that $N_1 = a_1 = \rho a_2 > 1$, it holds that:*

$$\mathcal{L}_{\mathrm{SC}} \geq f(\cos(\theta_1), \cos(\theta_2)), \tag{3}$$

where $f(\cdot): \mathbb{R} \times \mathbb{R} \to \mathbb{R}$ is defined as:

$$\begin{aligned} f(x_1, x_2) = {} & \rho a_2 \log\left((\rho a_2 - 1) + e^{-1}(K-1)\, a_2 \exp(x_1)\right) \\ & + (K-1) a_2 \log\left((a_2 - 1) + e^{-1}\left((K-2)\, a_2 \exp(x_2) + \rho a_2 \exp(x_1)\right)\right), \end{aligned} \tag{4}$$

and equality is attained if and only if there exists a configuration of $\bar{Z} = (\bar{z}_1, \ldots, \bar{z}_K) \in (\mathbb{S}^{h-1})^K$ such that:

(A3) $i \in B_k$, $z_i = \bar{z}_k$.

(A4) $\forall k, k' \in \{2, \ldots, K\}$ *and* $k \neq k'$, $\langle \bar{z}_1, \bar{z}_k \rangle = \cos(\theta_1)$, $\langle \bar{z}_k, \bar{z}_{k'} \rangle = \cos(\theta_2)$, *and* $\cos(\theta_2) = \frac{(K-1)\cos^2(\theta_1) - 1}{K-2}$.

(A5) (Case 1) $\rho < 1$: $\theta_1 \in \left(\cos^{-1}(-\frac{1}{K-1}), 0\right)$ *such that* $f'_{x_1}(\cos(\theta_1)) = 0$.

(Case 2) $\rho = 1$: $\theta_1 = \cos^{-1}(-\frac{1}{K-1})$.

(Case 3) $1 < \rho < R(K, a_2)$: $\theta_1 \in \left(-\pi, \cos^{-1}(-\frac{1}{K-1})\right)$ *such that* $f'_{x_1}(\cos(\theta_1)) = 0$.

(Case 4) $\rho \geq R(K, a_2)$: $\theta_1 = -\pi$.

Let $b_1 = (K-1)(1+e^{-2}-2e^2)a_2 - 2$, $b_2 = 8(1+e^{-2})(K-1)a_2((K-1)a_2 - e^2)$, then $R(K, a_2)$ defined as:

$$R(K, a_2) = \frac{-b_1 + \sqrt{b_1^2 + b_2}}{2(1+e^{-2})a_2}. \tag{5}$$

The proof is provided in Appendix B.2. We show that x_2 is dependent on x_1 and then f becomes a convex function of x_1. f'_{x_1} is an increasing function of ρ. Thus, f has one and only one minimal

value within a domain with $f_{\text{min}} = f(\cos(\theta_1))$. As ρ increases, θ_1 increases and θ_2 decreases. θ_1 measures the extent of dominance of the head class in the feature space.

Remark 2. *$R(K, a_2)$ in Eq. (5) can be roughly simplified as a linear function only respect to K:*

$$R'(K) = (K-1)\frac{-(1+e^{-2}-2e^2)+\sqrt{(1+e^{-2}-2e^2)^2+8(1+e^{-2})}}{2(1+e^{-2})} \approx 12.16(K-1) \quad (6)$$

$R'(K)$ provides an approximate estimate to distinguish Case 3 and Case 4 in Theorem 2.

Numerical Examples. To quantify the extent that long-tailed data skews the feature space, we consider two examples with $K = 3$ classes. The tail-classes have $N_2 = N_3 = 50$ samples. In Example A, $\rho_A = 10$, and the head class has $N_1^A = 500$ samples. In Example B, $\rho_B = 100$, so $N_1^B = 5000$. $\rho_A < R'(3) < \rho_B$. All samples are mapped to a unit circle ($\mathbb{S}^1$). Then $\theta_1^A = 149.19°$, $\theta_2^A = 61.63°$, $\theta_1^B = 180°$ and $\theta_2^B = 0°$ can be found when f is minimized. Fig. 2 visualizes values of the lower bound function f and the empirical representations of both examples.

4 METHOD

4.1 CHALLENGES IN LONG-TAILED REPRESENTATION LEARNING

Skewed Center Configuration. Theorem 2 reveals that long-tailed data forces tail classes' centers to shrink or even collapse. We refer to this phenomenon as the skewed center configuration. This leads to the feature distributions of the tail classes partially (Fig. 2c) or fully (Fig. 2d) overlapping. As a result, samples in the overlapping regions become inseparable and cannot be distinguished by a classifier.

Distribution Shift. One may consider rearranging the center configuration to symmetric one to separate the overlapping features. This approach implicitly assumes that the distribution of training data, $\mathcal{P}_{\text{train}}$, is the same with the true distribution of the underlying data, $\mathcal{P}_{\text{true}}$. However, due to the limited sample sizes of tail classes, a discrepancy often exists between $\mathcal{P}_{\text{train}}$ and $\mathcal{P}_{\text{true}}$. We refer to this phenomenon as distribution shift. When it occurs, rearranging the training center configuration can separate the training data but cannot ensure the separation of testing data and may even causes overlapping distributions between head and tail classes (as depicted in Fig. 3).

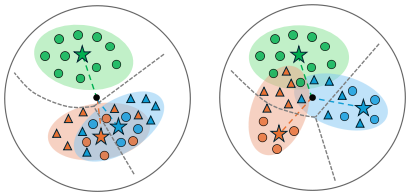

Figure 3: long-tailed data representations. Left: Before center correction. Right: After center correction with distribution shifts. To save space, we defer the legend to Fig. 4.

4.2 FEATRECON

To address the problems that are discussed above, we design our method to reconstruct the feature space of long-tailed data to be both symmetric and linearly separable.

Theorem 2 suggests that balancing sample size can correct the center configuration. To achieve this, we directly generate synthetic features in the feature space. Since all features are normalized (i.e, $Z \in \mathbb{S}^{h-1}$), it is reasonable to assume that the features of each class fall within a hyperspherical cap on $\mathbb{S}^{h-1}$, parameterized by a center and a "radius" – a fixed central angle. Thus, for each class, we estimate its confidence support as a hyperspherical cap that contains the majority of features. We then uniformly sample synthetic features from these supports. Each support is filled with real and synthetic features, and features from nearby classes are pushed away as training progresses.

However, since tail classes have limited sample sizes, their estimated supports are unreliable. To prevent missing features of tail classes from falling outside their respective supports and overlapping with the features of the head classes, we regularize tail classes' estimation with the statistics of neighboring head classes. Since the synthetic samples ensure the learnt representation configuration to be symmetric, as long as the central angle of any confidence support is sufficiently small (at the most $\frac{1}{2}\cos^{-1}(-\frac{1}{K-1})$), these confidence supports are guaranteed to be linearly separable.

The procedure is illustrated in Fig. 4. In Fig. 4a, we estimate the confidence support based on limited training samples. In Fig. 4b, the confidence supports of tail classes are regularized using the head

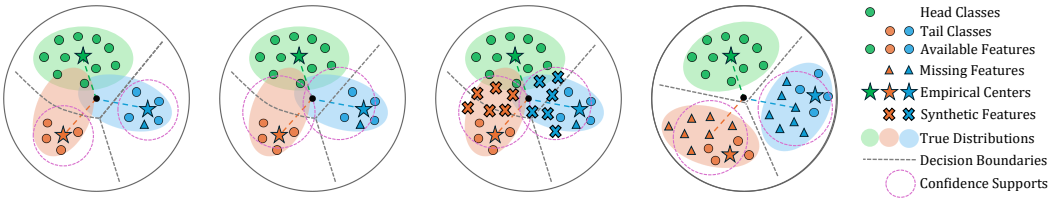

(a) (b) (c) (d)

Figure 4: One iteration of our algorithm. (a) Estimation of the confidence supports with training data. The supports are drawn in dashed magenta circles. (b) Regularization of the support by head class statistics. (c) Generating synthetic features to fill the supports (cross markers). (d) Optimization of the SC loss separates the tail classes and their supports.

class statistics. In Fig. 4c, we generate synthetic samples filling these confidence supports. Finally, by minimizing the SC loss, class centers are moved to equal distance from each other, and the supports are guaranteed to be linearly separable (Fig. 4d). In practice, we repeat the procedure iteratively.

Confidence Supports Estimation. A hyperspherical cap can be characterized by its center and a central angle. For class k, we estimate these parameters as follows:

$$\hat{\mu}_k = \frac{1}{N_k} \sum_{i \in B_k} z_i, \text{ and } \hat{\theta}_k = Q_\alpha \{\cos^{-1}(z_i \cdot \hat{\mu}_k) | y_i = k\}, \tag{7}$$

where Q_α denotes the α quantile. Normalization is applied wherever necessary to keep the center estimator a unit vector.

Head Class Regularization. For tail classes, the statistics are regularized using the statistics of $\mathcal{P}_{\text{true}}$ from head classes, which are estimated more accurately due to sufficient training samples. This improves the robustness of tail class parameter estimation. Specifically, for a tail class k, we select the top q head classes ($\mathcal{C}_h$) with the highest similarities to its class center $\hat{\mu}$:

$$\mathcal{C}_k^q = \left\{ i \mid \hat{\mu}_i \cdot \hat{\mu}_k \in \text{top}_q \left(\mathcal{S}_k \right) \right\}, \text{ where } \mathcal{S}_k = \left\{ \hat{\mu}_i \cdot \hat{\mu}_k \mid i \in \mathcal{C}_h \right\}, \tag{8}$$

and regularize its statistics using those from the selected head classes ($\mathcal{C}_k^q$) as follows:

$$\hat{\mu}'_k = (1-\gamma) \sum \omega_k^c \hat{\mu}_c + \gamma \hat{\mu}_k \text{ and } \hat{\theta}'_k \quad = (1-\gamma) \sum \omega_k^c \hat{\theta}_c + \gamma \hat{\theta}_k \tag{9}$$

where $\omega_k^c = \frac{\hat{\mu}_i \cdot \hat{\mu}_k}{\sum_{j \in \mathcal{C}_k^q} \hat{\mu}_i \cdot \hat{\mu}_j}$ is the regularization weight of class c, and γ is the regularization magnitude.

Feature Generation. The estimated confidence support of class k is defined as the set of points:

$$\tilde{\mathcal{Z}}_k = \left\{ \tilde{z} \in \mathbb{S}^{h-1} \mid \tilde{z}^\top \hat{\mu}'_k \geq \cos(\bar{\theta}_k) \right\}, \text{ where } \bar{\theta}_k = \min\{\hat{\theta}'_k, \frac{1}{2} \cos^{-1}(-\frac{1}{K-1})\}. \tag{10}$$

Let $N_{\text{max/min}} = \max/\min\{N_k : k \in [K]\}$, we uniformly sample $mN_{\text{max}} - N_k$ points from $\tilde{\mathcal{Z}}_k$ as the synthetic features for class k, where m controls the total number of synthetic features.

Temperature Adjustment. Previous works (Kukleva et al., 2023) have revealed that τ in the InfoNEC (Wu et al., 2018) loss controls the preference between intra-class and inter-class discrimination. Head classes benefit from a larger τ while tail classes benefit from a smaller one. We demonstrate (in Appendix A.3.2) it holds for SC loss too. Inspired by this, we adjust temperature for class k as:

$$\tau_k = \left(1 - 0.5 \left(1 + \cos \left(\pi \frac{N_k - N_{\text{min}}}{N_{\text{max}} - N_{\text{min}}} \right) \right) \right) \times (\tau_+ - \tau_-) + \tau_- \tag{11}$$

where τ_+, τ_- denote the upper and lower bounds of τ, respectively.

Additionally, gradient analysis (in Appendix A.3.1) shows that τ also controls the gradient scale: the larger the τ, the smaller the gradient. Therefore, we re-balance the gradient scale of samples by class via adjusting the weight of $\mathcal{L}_{SC}^{k,i}$, and modify the SC loss as follows:

$$\mathcal{L}_{\text{SC}} = \sum_{k=1}^{K} \sum_{i \in B_k} \frac{\tau_k}{\tau_-} \mathcal{L}_{\text{SC}}^{k,i} \tag{12}$$

Table 1: Top-1 accuracy of ResNet-32 on CIFAR-10/100-LT datasets with different imbalance factors.

Dataset	CIFAR-10-LT			CIFAR-100-LT		
Imbalance Ratio (ρ)	100	50	10	100	50	10
CE	70.36	74.81	86.39	38.32	43.85	55.71
Focal Loss (Lin et al., 2017)	70.38	76.72	86.66	38.41	44.32	55.78
CB-Focal (Cui et al., 2019)	74.57	79.27	87.10	39.60	45.17	57.99
LDAM-DRW (Cao et al., 2019)	77.03	81.03	88.16	42.04	46.62	58.71
CB-DA-LDAM (Jamal et al., 2020)	80.00	82.23	87.40	44.08	49.16	58.00
CE-OTmix (Gao et al., 2024)	78.30	83.40	90.20	46.40	40.70	61.60
DWR-OTmix (Cao et al., 2019; Gao et al., 2024)	83.10	86.40	90.60	48.00	52.60	62.70
SCL (Khosla et al., 2020) -	-	-	-	42.10	45.20	54.80
Hybrid-SC (Wang et al., 2021)	81.40	85.36	91.12	46.72	51.87	63.05
Hybrid-PSC (Wang et al., 2021)	78.82	83.86	90.96	44.97	48.93	62.70
KCL (Kang et al., 2021)	77.60	81.70	88.00	42.80	46.30	57.60
TSC (Li et al., 2022)	79.70	82.90	88.70	43.80	47.40	59.00
BCL (Zhu et al., 2022)	84.32	87.24	91.12	51.93	56.59	64.87
SBCL (Hou et al., 2023) -	-	-	-	44.90	48.70	57.90
FeatRecon	**86.42**	**88.49**	**92.03**	**53.41**	**57.48**	**65.67**

Training Framework. Our training framework mainly follows (Zhu et al., 2022; Du et al., 2024). The model consists of: 1) a base encoder $f : X \to h$ that extracts latent embeddings; 2) a prediction head $l : h \to p$ that produces model predictions $p = l \circ f(\mathcal{X})$; 3) a projection head $g : h \to z$ that generates normalized representations $z = g \circ f(\mathcal{X})$.

The prediction head is optimized using the training data with the cross entropy loss and logit compensation (Menon et al., 2021). Let $\mathbb{P}(y)$ be class priors and $\delta_y = \log \mathbb{P}_y$. Then the $\mathcal{L}_x$ is:

$$\mathcal{L}_x(y, l \circ f(x)) = -\log \frac{\exp\left(p_y + \delta_y\right)}{\sum_{y' \in [\mathcal{Y}]} \exp\left(p_{y'} + \delta_{y'}\right)} \tag{13}$$

The projection head is optimized with both real and synthetic features with the supervised contrastive loss $\mathcal{L}_{SC}$. The final objective is:

$$\mathcal{L} = \lambda_x \mathcal{L}_x + \lambda_c \mathcal{L}_{SC} \tag{14}$$

where λ_x and λ_c are hyperparameters that control relative strength among different losses.

5 Experiments

5.1 Dataset and Implementation Details.

Dataset. CIFAR-10-LT and CIFAR-100-LT are the imbalanced subsets of the original CIFAR-10 and CIFAR-100 (Krizhevsky et al., 2009), following (Kang et al., 2021; Li et al., 2022; Zhu et al., 2022). We set the imbalance factor $\rho = N_{max}/N_{min}$ to be 100, 50, and 10.

ImageNet-LT (Liu et al., 2019) is the subset of the original ImageNet (Deng et al., 2009), with the training set sampled with a Pareto distribution with power value α = 0.6 and testing set unchanged. The imbalance factor is 256, with the most frequent class having 1280 samples and the least frequent one having 5 samples.

iNaturalist 2018 (Van Horn et al., 2018) is a large-scale long-tailed dataset that contains 437.5K images from 8,142 classes with an extremely imbalanced distribution.

Table 2: Top-1 accuracy of ResNet-32 on CIFAR-100-LT with imbalance factor equaling 100.

	Methods	Many	Medium	Few	All
200 epochs	τ-norm (Kang et al., 2020)	61.4	42.5	15.7	41.4
	Hybrid-SC (Wang et al., 2021)	-	-	-	46.7
	DRO-LT (Samuel & Chechik, 2021)	64.7	50.0	23.8	47.3
	RIDE(3 experts) (Wang et al., 2020)	68.1	49.2	23.9	48.0
	BCL (Zhu et al., 2022)	67.2	53.1	32.9	51.9
	FeatRecon (Ours)	**69.2**	**53.3**	**35.0**	**53.4**
400 epochs	Balanced Softmax (Ren et al., 2020)	-	-	-	50.8
	PaCo (Cui et al., 2021)	-	-	-	52.0
	BCL (Zhu et al., 2022)	69.7	**53.8**	35.5	52.0
	FeatRecon (Ours)	**70.2**	**53.8**	**36.9**	**54.7**

Following previous works (Li et al., 2022; Zhu et al., 2022; Hou et al., 2023), we train our model on the long-tailed training sets and evaluate on the balanced testing sets. We divide the testing sets

Table 3: Top-1 accuracy of ResNet-50 on ImageNet-LT dataset and iNaturalist 2018 dataset.

Method	ImageNet-LT				iNaturalist 2018			
	Many	Med	Few	All	Many	Med	Few	All
CE	64.0	33.8	5.8	41.6	72.2	63.0	57.2	61.7
Focal Loss (Lin et al., 2017)	51.0	40.8	20.8	43.7	-	-	-	61.3
LDAM-DRW (Cao et al., 2019)	60.4	46.9	30.7	49.8	-	-	-	64.6
cRT (Kang et al., 2020)	58.8	44.4	26.1	47.3	69.0	66.0	63.2	65.2
τ-norm (Kang et al., 2020)	56.6	44.2	27.4	46.7	65.6	65.3	65.9	65.6
LWS (Kang et al., 2020)	57.1	45.2	29.3	47.7	65.0	66.3	65.5	65.9
Area (Chen et al., 2023)	-	-	-	49.5	-	-	-	68.4
CE-OTmix (Gao et al., 2024)	**70.0**	45.9	22.3	52.0	69.3	70.5	68.4	69.5
DRW-OTmix (Cao et al., 2019; Gao et al., 2024)	67.0	49.0	30.4	53.4	70.6	71.9	70.4	71.1
IWB (Dang et al., 2024)	64.2	52.2	40.2	55.2	72.3	70.6	72.5	71.5
SCL (Khosla et al., 2020)	61.4	47.0	28.2	49.8	-	-	-	66.4
KCL (Kang et al., 2021)	61.8	49.4	30.9	51.5				68.6
TSC (Li et al., 2022)	63.5	49.7	30.4	52.4	72.6	70.6	67.8	69.7
BCL (Zhu et al., 2022)	-	-	-	56.0	-	-	-	71.8
BCL (Zhu et al., 2022)	67.2	53.9	36.5	56.7	-	-	-	-
SBCL (Hou et al., 2023)	63.8	51.3	31.2	53.4	**73.3**	71.9	68.6	70.8
DecoupledCL (Xuan & Zhang, 2024)	68.5	55.2	35.4	57.7	**74.2**	72.9	70.3	72.0
Ours	68.1	**55.3**	**38.3**	**57.8**	72.0	**73.9**	**73.9**	**73.7**

into three subsets: many (with more than 100 instances), medium (with 20 to 100 instances), and few (with less than 20 instances) splits.

Implementation Details. To ensure a fair comparison, our implementation follows (Li et al., 2022; Zhu et al., 2022). For both CIFAR-10-LT and CIFAR-100-LT, we adopt the ResNet-32 as the backbone. The projection head is a 2-layer MLP that generates 128-dimensional embeddings. Dimension of the hidden layer is 512. Our model is trained for 200 epochs with a batch size of 256 and with a SGD optimizer. The momentum is 0.9 and the weight decay is $4e^{-4}$. The learning rate warms up 0.3 in the first 5 epochs and decay by 0.1 at the 160th and 180th epochs. For data augmentation, we adopt AutoAug (Cubuk et al., 2019) and Cutout (DeVries & Taylor, 2017) for the classification head, and adopt SimAug (Chen et al., 2020) for the projection head. For hyperparameters, we set $\lambda_c = 1$, $\lambda_c = 1$, $\alpha = 0.99$, and $\tau_- = 0.1$, $\tau_+ = 1$. We also train our model for 400 epochs for finer comparisons on CIFAR-100-LT. In this case, the learning rate warms up in the first 10 epochs and decay at the 360th and 380th epochs.

We adopt ResNet-50 (He et al., 2016) as the model backbone for both ImageNet-LT and iNaturalist 2018. The projection head is a 2-layer MLP that generates 1024-dimensional embeddings. Dimension of the hidden layer is 2048. For data augmentation, we switch the strategy for the projection head to RandAug (Cubuk et al., 2020). Our model is trained for 90 epochs for ImageNet-LT and 100 for iNaturalist 2018 epochs with a batch size of 256 and with a SGD optimizer. The momentum is 0.9 and the weight decay is $5e^{-4}$ for ImageNet-LT and $1e^{-4}$ for iNaturalist 2018. The learning rate is 0.1 for ImageNet-LT and 0.2 for iNaturalist 2018 with a cosine scheduler. Additionaly, we train our model for 90 epochs using ResNeXt-50-32x4d (Xie et al., 2017) as the backbone. For hyperparameters, we set $\lambda_c = 1$, $\lambda_c = 1$, $\alpha = 0.99$, and $\tau_- = 0.07$, $\tau_+ = 1$.

5.2 Results

CIFAR-LT Tab. 1 shows experiment results on CIFAR-10/100-LT datasets with imbalance factor varying among 10, 50, and 100. For baselines, we select methods that only work with classifiers (Lin et al., 2017; Cui et al., 2019; Cao et al., 2019; Jamal et al., 2020; Gao et al., 2024) and methods that work with both representations and classifiers (Khosla et al., 2020; Wang et al., 2021; Kang et al., 2021; Li et al., 2022; Zhu et al., 2022; Hou et al., 2023). We can see that FeatRecon outperforms baseline models in all settings. Moreover, our model achieves larger performance gain as the imbalance factor increases, proving the effectiveness of our method for long-tailed data. Additionally, in Tab. 2, we provide shot-wise results on CIFAR-100-LT data with imbalance factor of 100. The model is trained for both 200 epochs and 400 epochs for fair comparisons with baselines that are

trained under different settings. The results demonstrate the superiority of our approach, especially for the few-shot classes.

ImageNet-LT Tab. 3 shows experiment results on ImageNet-LT dataset using ResNet-50 as model backbone. Tab. 4 shows experiment results using ResNeXt-50 as model backbone. We report the overall Top-1 accuracy as well as the Top-1 accuracy on Many-shot, Medium-shot, and Few-shot classes. Similar to the experiments on CIFAR-LT, we select methods that only work with classifiers (Lin et al., 2017; Cao et al., 2019; Kang et al., 2020; Chen et al., 2023; Gao et al., 2024; Dang et al., 2024) and methods that work with both representations and classifiers (Khosla et al., 2020; Kang et al., 2021; Li et al., 2022; Zhu et al., 2022; Hou et al., 2023; Xuan & Zhang, 2024) for baselines. Results show that our method outperforms baselines on the accuracy of tail classes and overall accuracy, demonstrating the effectiveness of our approach for learning classes with missing samples.

Table 4: Top-1 accuracy of ResNeXt-50 on ImageNet-LT dataset.

Method	Many	Med	Few	All
Focal Loss (Lin et al., 2017)	64.3	37.1	8.2	43.7
τ-norm (Kang et al., 2020)	59.1	46.9	30.7	49.4
LWS (Kang et al., 2020)	60.2	47.2	30.3	49.9
IWB (Dang et al., 2024)	64.2	52.2	40.2	55.2
BCL (Zhu et al., 2022)	67.2	53.9	36.5	56.7
Ours	**68.7**	**55.6**	**38.6**	**58.3**

iNaturalist 2018 Tab. 3 also lists experiment results on iNaturalist 2018 dataset. Similar to results on ImageNet-LT, our method outperforms baselines on the accuracy of tail classes and overall accuracy, highlighting our model's capability of learning from few samples.

5.3 Ablation Study

We evaluate the design of FeatRecon through an ablation study on CIFAR-100-LT dataset, with an imbalance factor of 100. Each model runs for 400 epochs. Results are displayed in Tab. 5. Exp. 1 provides the baseline by training a classifier with logit compensation (LP) (Menon et al., 2021). Exp. 2 introduces an additional projection head and trains feature representations with the SC loss (Khosla et al., 2020). This design brings a 1.6% performance improvement, underscoring the benefit of representation learning. In Exp. 3, we balance the sample size across different classes by naively upsampling (Up Sam) the existing features for representation learning. However, this approach has no positive effect. It highlights the effectiveness of our synthetic feature generation method (Feat Gen), shown in Exp. 4, that brings a 3.1% performance gain. In Exp. 5, we validate the benefit of training with temperature adjustment (Temp Adj), which leads to an additional 1.1% performance increase.

Table 5: Ablating model components.

Exp	LC	SC	Up Sam	Feat Gen	Temp Adj	Accuracy	Δ
1	✓					50.8	
2	✓	✓				52.4	+1.6
3	✓	✓	✓			52.6	+1.8
4	✓	✓		✓		53.9	+3.1
5	✓	✓		✓	✓	**55.0**	**+4.2**

6 Conclusion and Limitations

In this paper, we establish a theoretical framework to investigate the optimal representation configuration for long-tailed data and prove that the centers of the tail classes are forced to shrink and even collapse. Following the analysis, we study the problem behinds the long-tailed representation learnt via optimizing the supervised contrastive loss and identify two challenges, the skewed center configuration and distribution shifts. Inspired by our analysis, we introduce a novel method for long-tailed representation learning. Our methods reconstructs feature space for long tail data so that representations of each class are arranged into symmetric and linearly separable areas. We demonstrate the effectiveness of our methods on different benchmark datasets. And results show that our method achieves state-of-the-art performances.

While our theoretical framework opens a door to study long-tailed representation, it's currently limited to the simple one vs all case. The solution for more general cases remains unsolved.

REFERENCES

Sumyeong Ahn, Jongwoo Ko, and Se-Young Yun. Cuda: Curriculum of data augmentation for long-tailed recognition. *ICLR*, 2023.

Jonathon Byrd and Zachary Lipton. What is the effect of importance weighting in deep learning? In *International conference on machine learning*, pp. 872–881. PMLR, 2019.

Kaidi Cao, Colin Wei, Adrien Gaidon, Nikos Arechiga, and Tengyu Ma. Learning imbalanced datasets with label-distribution-aware margin loss. In *NeurIPS*, 2019.

Mathilde Caron, Ishan Misra, Julien Mairal, Priya Goyal, Piotr Bojanowski, and Armand Joulin. Unsupervised learning of visual features by contrasting cluster assignments. In *NeurIPS*, 2020.

Jiahao Chen and Bing Su. Transfer knowledge from head to tail: Uncertainty calibration under long-tailed distribution. In *CVPR*, 2023.

Ting Chen, Simon Kornblith, Mohammad Norouzi, and Geoffrey Hinton. A simple framework for contrastive learning of visual representations. In *ICML*, 2020.

Xiaohua Chen, Yucan Zhou, Dayan Wu, Chule Yang, Bo Li, Qinghua Hu, and Weiping Wang. Area: adaptive reweighting via effective area for long-tailed classification. In *CVPR*, 2023.

Xinlei Chen and Kaiming He. Exploring simple Siamese representation learning. In *CVPR*, 2021.

Ekin D Cubuk, Barret Zoph, Dandelion Mane, Vijay Vasudevan, and Quoc V Le. Autoaugment: Learning augmentation strategies from data. In *CVPR*, 2019.

Ekin D Cubuk, Barret Zoph, Jonathon Shlens, and Quoc V Le. Randaugment: Practical automated data augmentation with a reduced search space. In *CVPR workshops*, 2020.

Jiequan Cui, Zhisheng Zhong, Shu Liu, Bei Yu, and Jiaya Jia. Parametric contrastive learning. In *ICCV*, 2021.

Yin Cui, Menglin Jia, Tsung-Yi Lin, Yang Song, and Serge Belongie. Class-balanced loss based on effective number of samples. In *CVPR*, 2019.

Wenqi Dang, Zhou Yang, Weisheng Dong, Xin Li, and Guangming Shi. Inverse weight-balancing for deep long-tailed learning. In *AAAI*, 2024.

Philippe Delsarte, Jean-Marie Goethals, and Johan Jacob Seidel. Spherical codes and designs. In *Geometry and Combinatorics*. Elsevier, 1977.

Jia Deng, Wei Dong, Richard Socher, Li-Jia Li, Kai Li, and Li Fei-Fei. Imagenet: A large-scale hierarchical image database. In *CVPR*, 2009.

Terrance DeVries and Graham W Taylor. Improved regularization of convolutional neural networks with cutout. *arXiv*, 2017.

Chaoqun Du, Yulin Wang, Shiji Song, and Gao Huang. Probabilistic contrastive learning for long-tailed visual recognition. *TPAMI*, 2024.

Jintong Gao, He Zhao, Zhuo Li, and Dandan Guo. Enhancing minority classes by mixing: An adaptative optimal transport approach for long-tailed classification. *NeurIPS*, 2024.

Florian Graf, Christoph Hofer, Marc Niethammer, and Roland Kwitt. Dissecting supervised contrastive learning. In *ICML*, 2021.

Jean-Bastien Grill, Florian Strub, Florent Altché, Corentin Tallec, Pierre Richemond, Elena Buchatskaya, Carl Doersch, Bernardo Avila Pires, Zhaohan Guo, Mohammad Gheshlaghi Azar, et al. Bootstrap your own latent a new approach to self-supervised learning. In *NeurIPS*, 2020.

Kaiming He, Xiangyu Zhang, Shaoqing Ren, and Jian Sun. Deep residual learning for image recognition. In *CVPR*, 2016.

Kaiming He, Haoqi Fan, Yuxin Wu, Saining Xie, and Ross Girshick. Momentum Contrast for Unsupervised Visual Representation Learning. In *CVPR*, 2020.

Chengkai Hou, Jieyu Zhang, Haonan Wang, and Tianyi Zhou. Subclass-balancing contrastive learning for long-tailed recognition. In *ICCV*, 2023.

Muhammad Abdullah Jamal, Matthew Brown, Ming-Hsuan Yang, Liqiang Wang, and Boqing Gong. Rethinking class-balanced methods for long-tailed visual recognition from a domain adaptation perspective. In *CVPR*, 2020.

Bingyi Kang, Saining Xie, Marcus Rohrbach, Zhicheng Yan, Albert Gordo, Jiashi Feng, and Yannis Kalantidis. Decoupling representation and classifier for long-tailed recognition. In *ICLR*, 2020.

Bingyi Kang, Yu Li, Sa Xie, Zehuan Yuan, and Jiashi Feng. Exploring balanced feature spaces for representation learning. In *ICLR*, 2021.

Salman Khan, Munawar Hayat, Syed Waqas Zamir, Jianbing Shen, and Ling Shao. Striking the right balance with uncertainty. In *CVPR*, 2019.

Prannay Khosla, Piotr Teterwak, Chen Wang, Aaron Sarna, Yonglong Tian, Phillip Isola, Aaron Maschinot, Ce Liu, and Dilip Krishnan. Supervised contrastive learning. In *NeurIPS*, 2020.

Alex Krizhevsky, Geoffrey Hinton, et al. Learning multiple layers of features from tiny images. 2009.

Anna Kukleva, Moritz Böhle, Bernt Schiele, Hilde Kuehne, and Christian Rupprecht. Temperature schedules for self-supervised contrastive methods on long-tail data. In *ICLR*, 2023.

Tianhong Li, Peng Cao, Yuan Yuan, Lijie Fan, Yuzhe Yang, Rogerio S Feris, Piotr Indyk, and Dina Katabi. Targeted supervised contrastive learning for long-tailed recognition. In *CVPR*, 2022.

Tsung-Yi Lin, Priya Goyal, Ross Girshick, Kaiming He, and Piotr Dollár. Focal loss for dense object detection. In *ICCV*, 2017.

Ziwei Liu, Zhongqi Miao, Xiaohang Zhan, Jiayun Wang, Boqing Gong, and Stella X Yu. Large-scale long-tailed recognition in an open world. In *CVPR*, 2019.

Aditya Krishna Menon, Sadeep Jayasumana, Ankit Singh Rawat, Himanshu Jain, Andreas Veit, and Sanjiv Kumar. Long-tail learning via logit adjustment. In *ICLR*, 2021.

Jiawei Ren, Cunjun Yu, Xiao Ma, Haiyu Zhao, Shuai Yi, et al. Balanced meta-softmax for long-tailed visual recognition. *NeurIPS*, 2020.

Dvir Samuel and Gal Chechik. Distributional robustness loss for long-tail learning. In *CVPR*, 2021.

Laurens Van Der Maaten and Geoffrey Hinton. Visualizing data using t-SNE. *JMLR*, 2008.

Grant Van Horn, Oisin Mac Aodha, Yang Song, Yin Cui, Chen Sun, Alex Shepard, Hartwig Adam, Pietro Perona, and Serge Belongie. The inaturalist species classification and detection dataset. In *CVPR*, 2018.

Peng Wang, Kai Han, Xiu-Shen Wei, Lei Zhang, and Lei Wang. Contrastive learning based hybrid networks for long-tailed image classification. In *CVPR*, 2021.

Tongzhou Wang and Phillip Isola. Understanding contrastive representation learning through alignment and uniformity on the hypersphere. In *ICML*, 2020.

Xudong Wang, Long Lian, Zhongqi Miao, Ziwei Liu, and Stella X Yu. Long-tailed recognition by routing diverse distribution-aware experts. *arXiv*, 2020.

Zhirong Wu, Yuanjun Xiong, Stella X. Yu, and Dahua Lin. Unsupervised Feature Learning via Non-parametric Instance Discrimination. In *CVPR*, 2018.

Saining Xie, Ross Girshick, Piotr Dollár, Zhuowen Tu, and Kaiming He. Aggregated residual transformations for deep neural networks. In *CVPR*, 2017.

Shiyu Xuan and Shiliang Zhang. Decoupled contrastive learning for long-tailed recognition. In *AAAI*, 2024.

Manyi Zhang, Xuyang Zhao, Jun Yao, Chun Yuan, and Weiran Huang. When noisy labels meet long tail dilemmas: A representation calibration method. In *CVPR*, 2023.

Jianggang Zhu, Zheng Wang, Jingjing Chen, Yi-Ping Phoebe Chen, and Yu-Gang Jiang. Balanced contrastive learning for long-tailed visual recognition. In *CVPR*, 2022.

A APPENDIX A

A.1 PSEUDO ALGORITHMS

In this section, we first present the pseudo algorithms of FeatRecon. FeatRecon is a heuristic method that iteratively generates synthetic features, adjust representations, and re-estimate confidence supports at each step of the training process.

Algorithm 1: FeatRecon Algorithm

Input: Available training samples $\{x_i, y_i\}_{i \in B_k, k \in [K]}$ from K classes, the quantile parameter α, the regularization magnitude γ and m which controls the total number of synthetic features.

```
for t = 1, ..., T do
    for k = 1, ..., K do
        Estimate confident supports for class k as Eq. (9) and Eq. (10) ;
        if class k is a tail class then
            Regularize its statistics as Eq. (9);
        end
        Generate mN_max − N_k synthetic features for class k ;
    end
    Compute the cross entropy loss L_x (Eq. (13)) with training data ;
    Compute the supervised contrastive loss L_SC (Eq. (12)) with both real features and synthetic features ;
    Update model with loss L = λ_x L_x + λ_c L_SC ;
end
Return Trained model
```

A.2 MORE EXPLANATION OF THEOREM 2

In this subsection, we provide more detailed mathematical explanation with respect to Theorem 2.

It states the necessary and sufficient conditions on the representation configuration for the SC loss attaining its minimal. (A3) states representations of each class converge to the respective class centers. (A4) states that the centers of class 2 to K form an $K-2$ equidistant simplex, the angles between whose vertices all equal θ_2. (A4) also states the vector between the spherical center and the center of class 1 is perpendicular to the equidistant simplex, and the angle between class 1's center and other classes' center all equal θ_1. And $\cos(\theta_2) = \frac{(K-1)\cos^2(\theta_1)-1}{K-2}$. (A5) depicts the whole dynamic of the configuration of all centers as ρ increases from 0 to $+\infty$.

More specifically, (A5) shows:

(Case 1) $0 < \rho < 1$: $\frac{\pi}{2} < \theta_1 < \cos^{-1}(-\frac{1}{K-1}) < \theta_2 < \cos^{-1}(-\frac{1}{K-2})$

(Case 2) $\rho = 1$: it becomes a data balance case where $\theta_1 = \theta_2 = \cos^{-1}(-\frac{1}{K-1})$. This indicates all class centers form a $K-1$ regular simplex.

(Case 3) $1 < \rho < R(K, a_2)$: as ρ continues to increase, it becomes a long-tailed problem. The head class (1^{st}) increasingly dominates the feature space as $\pi > \theta_1 > \cos^{-1}(-\frac{1}{K-1}) > \theta_2 > 0$. At this stage, the centers of the tail classes increasingly shrinks together.

(Case 4) $\rho > R(K, a_2)$: the centers of the tail classes collapses with $\theta_2 = 0$ and $\theta_1 = \pi$

In both long-tailed cases, θ_1 measures the extent that a head class dominate the feature space. Also, Theorem 1 is a special case of Theorem 2 (Case 2).

A.3 Role of Temperature in the SC loss

In this section, we show that the temperature parameter τ controls the scale of the gradient of the supervised contrastive loss (SC loss). We also demonstrate that τ controls the preference between intra-class and inter-class discrimination for the SC loss in the same way it does for the InfoNEC loss. (discussed in (Kukleva et al., 2023)).

A.3.1 Gradient Deviation of Supervised Contrastive Loss

We first provide the gradient of the SC loss with respect to feature z_i. To do so, we define the contrastive probability of feature i from class k to feature m as:

$$\begin{aligned} p_{im} &= \frac{e^{s_{im}/\tau}}{e^{s_{im}/\tau} + \sum_{j \neq m} e^{s_{ij}/\tau}} \\ s_{im} &= z_i \cdot z_m. \end{aligned} \tag{15}$$

Then, the unnormalized supervised contrastive loss for sample i is:

$$\mathcal{L}_i = -\sum_{m \in B} y_{im} \cdot \log p_{im}, \text{ where } y_{im} = \mathbb{1}_{\{y_i = y_m\}}. \tag{16}$$

Now let's derive the gradient:

$$\frac{\partial p_{ik}}{\partial s_{ij}} = \frac{1}{\tau} \cdot \begin{cases} -p_{ik}^2 + p_{ik}, & j = k \\ -p_{ik} \cdot p_{ij}, & j \neq k, \end{cases} \tag{17}$$

$$\begin{aligned} \frac{\partial \mathcal{L}_i}{\partial s_{ij}} &= -\sum_k y_{ik} \cdot \frac{\partial \log p_{ik}}{\partial s_{ij}} = -\sum_k \frac{y_{ik}}{p_{ik}} \cdot \frac{\partial p_{ik}}{\partial s_{ij}} \\ &= -\frac{1}{\tau} \cdot y_{ij} \cdot (1 - p_{ij}) + \frac{1}{\tau} \cdot \sum_{k \neq j} \cdot y_{ik} \cdot p_{ij} \\ &= \frac{1}{\tau} \cdot (-y_{ij} + \sum_k \cdot y_{ik} \cdot p_{ij}) \\ &= \frac{1}{\tau} \cdot (p_{ij} - y_{ij}), \end{aligned} \tag{18}$$

$$\frac{\partial \mathcal{L}_i}{\partial z_i} = \sum_j \frac{\partial \mathcal{L}_i}{\partial s_{ij}} \cdot \frac{\partial s_{ij}}{\partial z_i} = \frac{1}{\tau} \{ \sum_j z_j \cdot (p_{ij} - y_{ij}) \}. \tag{19}$$

Since $\mathcal{L}_{\text{SC}}^{k,i} = \frac{\mathbb{1}_{\{N_k > 1\}}}{N_k - 1} \mathcal{L}_i$, the gradient of $\mathcal{L}_{\text{SC}}^{k,i}$ to feature z_i is:

$$\begin{aligned} \frac{\partial \mathcal{L}_{\text{SC}}^{k,i}}{\partial z_i} &= \frac{1}{\tau} \{ \sum_{j \in B_k \setminus \{i\}} z_j \cdot (p_{ij} - \frac{1}{N_k - 1}) + \sum_{j \in N(i)} z_j \cdot p_{ij} \} \\ &= \frac{1}{\tau} \{ - \sum_{j \in B_k \setminus \{i\}} \frac{z_j}{N_k - 1} + \sum_j z_j \cdot p_{ij} \} \end{aligned} \tag{20}$$

If we denote $\bar{Z}_k = \sum_{j \in B_k \setminus \{i\}} \frac{z_j}{N_k - 1}$ as the center of class k, then:

$$\frac{\partial \mathcal{L}_{\text{SC}}^{k,i}}{\partial z_i} = \frac{1}{\tau} \{ -\bar{Z}_k + \sum_j z_j \cdot p_{ij} \} \tag{21}$$

This reveals that for a given feature z_i. there are 1 attractive force from its class center $\bar{Z}_k$ and p_{ij} repulsive force from all other features. Eq. (21) also shows that the scale of the gradient of $\mathcal{L}_{\text{SC}}^{k,i}$ is inversely related to τ. If we set a different temperature τ_k for class k, the gradient becomes:

$$\frac{\partial \mathcal{L}_{\text{SC}}^{k,i}}{\partial z_i} = \frac{1}{\tau_k} \{ -\bar{Z}_k + \sum_j z_j \cdot p_{ij} \}. \tag{22}$$

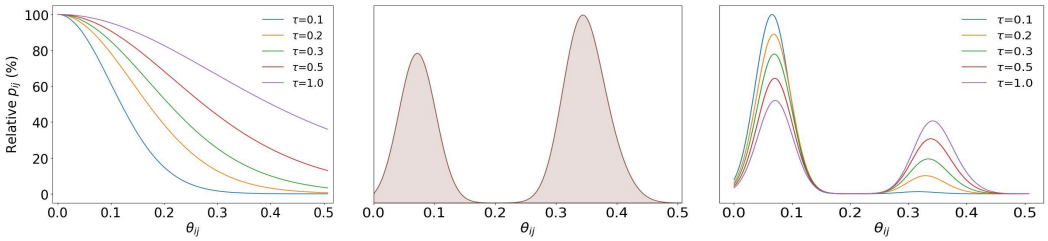

(a) (b) (c)

Figure 5: Role of temperature in the SC loss. a) The relationships between p_{ij} and θ_{ij}. Values are normalized for better comparison. b) The distribution of angles between z_i and all other features. c) Overall repulsive force from z_i at angle θ given τ. The left peak represents intra-class discrimination while the left peak represents inter-class discrimination.

To balance the gradient scale among different classes, we modify the loss function as follows:

$$\mathcal{L}^{k,i}_{\text{SC,modified}} = \frac{\tau_k}{\tau_-}\mathcal{L}^{k,i}_{\text{SC}}, \tag{23}$$

so that:

$$\frac{\partial \mathcal{L}^{k,i}_{\text{SC,modified}}}{\partial z_i} = \frac{1}{\tau_-}\{-\bar{Z}_k + \sum_j z_j \cdot p_{ij}\}. \tag{24}$$

Now the gradient scale becomes the same across different classes.

A.3.2 Temperature Controls Discrimination Preference

In this section, we study how τ controls the discrimination preference for the SC loss. Our analysis primarily follows the method proposed in (Kukleva et al., 2023).

All numerical examples are based on the representations of training samples of CIFAR-10 (Krizhevsky et al., 2009). And representations are learnt by a model trained via optimizing the SC loss, following the same experimental settings as in (Hou et al., 2023).

Since all features are normalized and $s_{ij} = \theta_{ij}$, Eq. (15) can be rewritten as:

$$p_{ij} = \frac{e^{\theta_{ij}/\tau}}{e^{\theta_{ij}/\tau} + \sum_{m \neq j} e^{\theta_{im}/\tau}}. \tag{25}$$

As indicated by Eq. (21), p_{ij} quantifies the magnitude of the repulsive force between z_i and z_j. Eq. (25) shows that this force is determined by their angular separation θ_{ij}. Denote $p_i(\theta, \tau)$ as a function of p_{ij} on θ_{ij} and τ. Fig. 5a depicts $p_i(\theta, \tau)$.

Denote $f_i(\theta)$ as the distribution density function of θ_{ij} for a feature z_i from class 0. Fig. 5b displays $f_i(\theta)$. The plot reveals two peaks: the left peak represents features from the same class, characterized by high similarities and small angles, whereas the right peak represents features from different classes, characterized by low similarities and large angles.

Denote $r_i(\theta, \tau)$ as the overall repulsive force of z_i at angle θ for a given temperature τ and $r_i(\theta, \tau)$ is defined as:

$$r_i(\theta, \tau) = p_i(\theta, \tau) \cdot f_i(\theta). \tag{26}$$

Fig. 5c depicts $r_i(\theta, \tau)$. The plot also reveals two peaks. The left peak represents the overall repulsive force from z_i towards features from the same class or indicative of the intra-class discrimination. The right peak represents the overall repulsive force from z_i towards features from different classes, or indicative of inter-class discrimination.

It is evident that a large τ favors inter-class discrimination while a small τ favors intra-class discrimination. Head classes benefit from inter-class discrimination, thereby a large τ. Tail classes benefit from intra-class discrimination, thereby a small τ (see more tails in (Kukleva et al., 2023)). This conclusion justifies our approach of adjusting temperature by class.

A.4 Additional Results (for Rebuttal)

In this sections, we provide additional results that are required by Reviewer 2QQJ and Reviewer MXe4.

A.4.1 Representation Visualization (for Reviewer 2QQJ)

In Fig. 6, we visualize the learned representations of CIFAR-10 testing images with imbalance factor equaling 100 using t-SNE (Van Der Maaten & Hinton, 2008). Results show that, with the help of synthetic features generated by FeatRecon, the resulting testing distributions of different classes are more separated.

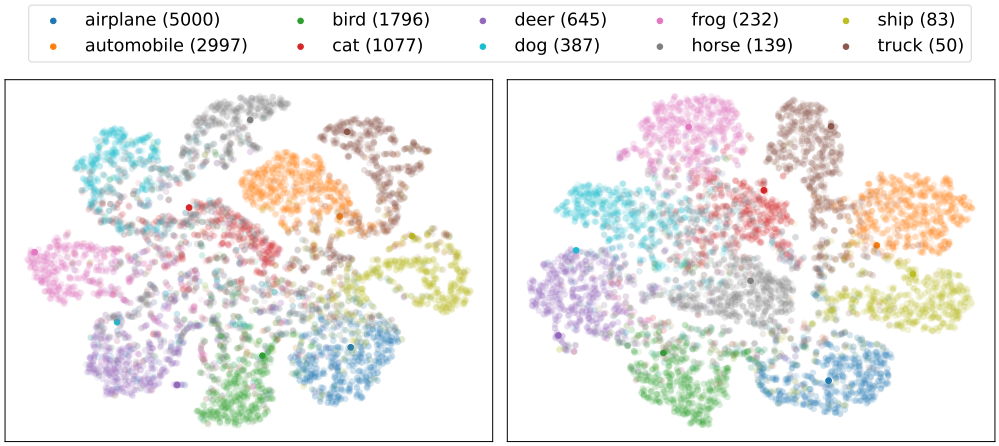

Figure 6: t-SNE visualization of CIFAR-10 testing set. (left) Learned representations without synthetic features. (Right) Learned representations with synthetic features generated by FeatRecon. Numbers in the legend after class names represents the numbers of training samples from this class.

A.4.2 Ablation Studies on q (for Reviewer MXe4)

We test sensitivity of hyper parameter q on regularization. Here we run an ablation study on CIFAR-100-LT dataset, with an imbalance factor of 100. Each model runs for 400 epochs. Results are displayed in Tab. 6, which indicates 30% classes should be used for regularization.

Table 6: Analysis of number of head classes for regularization q.

q	10	20	30	40
Accuracy	53.7	54.1	55.0	54.8

B APPENDIX B

B.1 PROOF OF THEOREM 1

In this section, we provide proofs for Theorem 1 proposed in Sec. 3.2. Our proof is different from what's shown in (Graf et al., 2021; Zhu et al., 2022) in order to take long-tailed distribution into account. For the convenience of your reading, let's recall some related notions and definitions.

- $h, N, K \in \mathbb{N}$
- $\mathcal{Z} = \mathbb{R}^h$
- $\mathbb{S}^{h-1} = \left\{z \in \mathbb{R}^h : \|z\| = 1\right\}$
- $\mathcal{Y} = \{1, \ldots, K\} = [K]$
- $B = \{1, \ldots, N\} = [N]$
- $B_k = \{i : i \in B, y_i = k\}$
- $N_k = |B_k|$

Definition 1 (Supervised contrastive loss) Let Z be an N point configuration (assuming all zs being normalized), $Z = (z_1, \ldots, z_N) \in (\mathbb{S}^{h-1})^N$, with labels $Y = (y_1, \ldots, y_N) \in ([K])^N$, and $K \leq h + 1$. Let $B = [N]$, $B_k = \{i : i \in B, y_i = k\}$ and $N_k = |B_k|$. The supervised contrastive loss $\mathcal{L}_{\mathrm{SC}}(\cdot; Y) : (\mathbb{S}^{h-1})^N \to \mathbb{R}$ is defined as:

$$\mathcal{L}_{\mathrm{SC}} = \sum_{k=1}^{K} \sum_{i \in B_k} \mathcal{L}_{\mathrm{SC}}^{k,i}, \text{ where } \mathcal{L}_{\mathrm{SC}}^{i} = -\frac{\mathbb{1}_{\{N_k > 1\}}}{N_k - 1} \sum_{j \in B_k \setminus \{i\}} \log \left(\frac{\exp\left(\langle z_i, z_j \rangle\right)}{\sum_{l \in B \setminus \{i\}} \exp\left(\langle z_i, z_l \rangle\right)} \right).$$

Definition 3 (Equidistant/regular Simplex) Let $h, K \in \mathbb{N}$ with $K \leq h + 1$. An K point configuration $\zeta = (\zeta_1, \ldots, \zeta_K) \in (\mathbb{S}^{h-1})^N$ form the vertices of an equidistant simplex inscribed in the unit-hypersphere, if and only if all of the following conditions hold:

(1) $\forall i \in [K], \|\zeta_i\| = 1$

(2) $\exists d \in \mathbb{R}, \forall i, j$ and $1 \leq i < j \leq K$, $d = \langle \zeta_i, \zeta_j \rangle$

And ζ form the vertices of a regular simplex inscribed in the unit-hypersphere, if and only if (1), (2) and the following condition holds:

(3) $\sum_{i \in [K]} \zeta_i = 0$

Theorem 1 Let Z be an N point configuration (assuming all zs being normalized), $Z = (z_1, \ldots, z_N) \in (\mathbb{S}^{h-1})^N$, with labels $Y = (y_1, \ldots, y_N) \in ([K])^N$, and $K \leq h + 1$. Let $B = [N]$, $B_k = \{i : i \in B, y_i = k\}$ and $N_k = |B_k|$. When Y is balanced, hence $\forall i \in [K]$, $N_k = \frac{N}{K}$, it holds that:

$$\mathcal{L}_{\mathrm{SC}} \geq N \log \left(\left(\frac{N}{K} - 1 \right) + \frac{N(K-1)}{K} \exp\left(-\frac{K}{K-1} \right) \right),$$

where equality is attained if and only if there exists a configuration of $\bar{Z} = (\bar{z}_1, \ldots, \bar{z}_K) \in (\mathbb{S}^{h-1})^K$ such that:

(A1) $i \in B_k$, $z_i = \bar{z}_k$.

(A2) $\bar{Z}$ form a regular simplex inscribed in the unit-hyperspher.

B.1.1 STEPS OF PROOF

First let's rewrite $\mathcal{L}_{\mathrm{SC}}^{k,i}$ and $\mathcal{L}_{\mathrm{SC}}$ (assuming $\forall k \in [K], N_k > 1$).

$$\begin{aligned}
\mathcal{L}_{\mathrm{SC}}^{k,i} &= -\frac{1}{N_k - 1} \sum_{j \in B_k \setminus \{i\}} \log \left(\frac{\exp\left(\langle z_i, z_j \rangle\right)}{\sum_{l \in B \setminus \{i\}} \exp\left(\langle z_i, z_l \rangle\right)} \right) \\
&= \frac{1}{N_k - 1} \sum_{j \in B_k \setminus \{i\}} \log \left(\frac{\sum_{l \in B \setminus \{i\}} \exp\left(\langle z_i, z_l \rangle\right)}{\exp\left(\langle z_i, z_j \rangle\right)} \right) \\
&= \frac{1}{N_k - 1} \log \left(\frac{\left(\sum_{l \in B \setminus \{i\}} \exp\left(\langle z_i, z_l \rangle\right) \right)^{N_k - 1}}{\prod_{j \in B_k \setminus \{i\}} \exp\left(\langle z_i, z_j \rangle\right)} \right) \\
&= \log \left(\frac{\sum_{l \in B \setminus \{i\}} \exp\left(\langle z_i, z_l \rangle\right)}{\exp\left(\sum_{j \in B_k \setminus \{i\}} \langle z_i, z_j \rangle \right)^{\frac{1}{N_k - 1}}} \right) \\
&= \log \left(\frac{\sum_{l \in B \setminus \{i\}} \exp\left(\langle z_i, z_l \rangle\right)}{\exp\left(\frac{1}{N_k - 1} \sum_{j \in B_k \setminus \{i\}} \langle z_i, z_j \rangle \right)} \right),
\end{aligned} \tag{27}$$

and hence

$$\begin{aligned}
\mathcal{L}_{\mathrm{SC}} &= \sum_{k=1}^{K} \sum_{i \in B_k} \mathcal{L}_{\mathrm{SC}}^{k,i} \\
&\overset{Lemma\ 2}{\geq} \sum_{k=1}^{K} N_k \log \left((N_k - 1) + e^{-1} \sum_{\substack{k' \in [K] \\ k' \neq k}} N_{k'} \exp\left(\langle \bar{z}_k, \bar{z}_{k'} \rangle\right) \right),
\end{aligned} \tag{28}$$

where $\bar{z}_k = \frac{1}{N_k} \sum_{i \in B_k} z_i$. When Y is balanced, $\forall i \in [K], N_k = \frac{N}{K}$, then

$$\begin{aligned}
\mathcal{L}_{\mathrm{SC}} &\geq \sum_{k=1}^{K} \frac{N}{K} \log \left(\left(\frac{N}{K} - 1 \right) + e^{-1} \frac{N}{K} \sum_{\substack{k' \in [K] \\ k' \neq k}} \exp\left(\langle \bar{z}_k, \bar{z}_{k'} \rangle\right) \right) \\
&\overset{Lemma\ 3}{\geq} N \log \left(\left(\frac{N}{K} - 1 \right) + e^{-1} \frac{N(K-1)}{K} \exp\left(\beta\right) \right),
\end{aligned} \tag{29}$$

and equality is attained if and only if all of the following conditions hold:

- (B1) $\forall i \in B_k$, $z_i = \bar{z}_k$.
- (B2) $\forall k \in [K]$ and $k' \in [K] \setminus \{k\}$, $\langle \bar{z}_k, \bar{z}_{k'} \rangle = \beta$.
- (B3) There exists a configuration of $\bar{Z} = (\bar{z}_1, \ldots, \bar{z}_K)$ such that (B2) holds.
  - (Case 1) $K = h + 1$: $\beta = -\frac{1}{K-1}$ or $\beta = 1$
  - (Case 2) $K < h + 1$: $-\frac{1}{K-1} \leq \beta \leq 1$

When $a, b > 0$, $f(x) = \log\left(a + be^x\right)$ is a strictly increasing function. And Eq. (29) suggests that the lower bound of $\mathcal{L}_{\mathrm{SC}}$ is a strictly increasing function of β. When β reaches its minimal value so does $\mathcal{L}_{\mathrm{SC}}$. When $K \leq h + 1$, $\beta_{\min} = -\frac{1}{K-1}$, then we have:

$$\begin{aligned}
\mathcal{L}_{\mathrm{SC}} &\geq N \log \left(\left(\frac{N}{K} - 1 \right) + e^{-1} \frac{N(K-1)}{K} \exp\left(-\frac{1}{K-1} \right) \right) \\
&= N \log \left(\left(\frac{N}{K} - 1 \right) + \frac{N(K-1)}{K} \exp\left(-\frac{K}{K-1} \right) \right).
\end{aligned} \tag{30}$$

When $\beta = -\frac{1}{K-1}$, Lemma 1 shows that (B2) and (B3) imply $\bar{Z} = (\bar{z}_1, \ldots, \bar{z}_K)$ form a regular simplex. Thus the conditions for equality can be sumerized as: there exists a configuration of $\bar{Z} = (\bar{z}_1, \ldots, \bar{z}_K) \in (\mathbb{S}^{h-1})^K$ such that:

(A1) $i \in B_k$, $z_i = \bar{z}_k$.

(A2) $\bar{Z}$ form a regular simplex inscribed in the unit-hyperspher.

B.1.2 LEMMAS PART 1

In this section,we provide definitions and proofs of lemmas that are used for the proof of Theorem 1.

Lemma 1. *Let Z be an K point configuration (assuming all zs being normalized), $Z = (z_1, \ldots, z_K) \in (\mathbb{S}^{h-1})^K$. If $\exists \beta \in \mathbb{R}$, $\forall i, j \in [K]$ and $i \neq j$ such that all inner products $\langle z_i, z_j \rangle = \beta$ are equal, then one of the following cases holds:*

(Case 1) $K > h + 1$: $\beta = 1$.

(Case 2) $K = h + 1$: $\beta = -\frac{1}{N-1}$ or $\beta = 1$.

(Case 3) $K < h + 1$: $-\frac{1}{N-1} \leq \beta \leq 1$.

And when $\beta = -\frac{1}{K-1}$, $Z = (z_1, \ldots, z_K)$ forms a regular simplex.

Proof. As explained in (Delsarte et al., 1977), there are at the most $h + 1$ equidistant points on $\mathbb{S}^{h-1}$ (The size of a spherical 1-distance set $\leq h+1$ (Delsarte et al., 1977)). When $N > h+1$, all N points collapse into a single point and $\beta = 1$, which is the Case 1. When $N = h + 1$, these points either form into a regular simplex or collapse into a single point, which is the Case 2. When $N < h + 1$, these points form into a regular/non-regular equidistant simplex or collapse into a single point, which is the Case 3.

Next we will show why when $K < h + 1$, $-\frac{1}{K-1} \leq \beta \leq 1$ (Case 3) and when $Z = (z_1, \ldots, z_K) \in (\mathbb{S}^{h-1})^K$ forms a regular simplex, $\beta = -\frac{1}{K-1}$ (Case 2). Given that

$$\begin{aligned} \left\| \sum_{k\in[K]} z_k \right\|^2 &= \left\langle \sum_{k\in[K]} z_k, \sum_{k\in[K]} z_k \right\rangle \\ &= \sum_{k\in[K]} \langle z_k, z_k \rangle + \sum_{\substack{n\in[K] \\ m\in[K]\setminus\{i\}}} \langle z_n, z_m \rangle \\ &= K + K(K-1)\beta \\ &\geq 0, \end{aligned} \tag{31}$$

this shows $-\frac{1}{K-1} \leq \beta$. Since β is the dot product of two unit vectors, $\beta \leq 1$. Then we have:

$$-\frac{1}{N-1} \leq \beta \leq 1. \tag{32}$$

When $Z = (z_1, \ldots, z_K) \in (\mathbb{S}^{h-1})^K$ forms a regular simplex, we have $\sum_{k\in[K]} z_k = 0$. Then $K + K(K-1)\beta = 0$ and $\beta = -\frac{1}{K-1}$.

Now we prove when $\beta = -\frac{1}{K-1}$, $Z = (z_1, \ldots, z_K)$ forms a regular simplex. Recall that $\forall i, j \in [K]$ and $i \neq j$, we have $\|z_i\| = 1$, and $\langle z_i, z_j \rangle = \beta$. When $\beta = -\frac{1}{K-1}$, Eq. (32) shows $\sum_{k\in[K]} z_k = 0$. Then Z forms a regular simplex. □

Lemma 2. *Let Z be an N point configuration (assuming all zs being normalized), $Z = (z_1, \ldots, z_N) \in (\mathbb{S}^{h-1})^N$, with labels $Y = (y_1, \ldots, y_N) \in ([K])^N$. Let $B = [N]$, $B_k = \{i :$*

$i \in B, y_i = k\}$. $\forall k \in [K]$, $\sum_{i \in B_k} \mathcal{L}_{\mathrm{SC}}^{k,i}$ *is bounded below by:*

$$\sum_{i \in B_k} \mathcal{L}_{\mathrm{SC}}^{k,i} \geq N_k \log \left((N_k - 1) + e^{-1} \sum_{\substack{k' \in [K] \\ k' \neq k}} N_{k'} \exp\left(\langle \bar{z}_k, \bar{z}_{k'} \rangle \right) \right), \tag{33}$$

where $\bar{z}_k = \frac{1}{N_k} \sum_{i \in B_k} z_i$*, and equality is attained if and only if the following condition holds:*

(B1) $\forall i \in B_k$, $z_i = \bar{z}_k$.

Proof. According to Eq. (27):

$$\begin{aligned} \mathcal{L}_{\mathrm{SC}}^{k,i} &= \log \left(\frac{\sum_{l \in B \setminus \{i\}} \exp\left(\langle z_i, z_l \rangle \right)}{\exp\left(\frac{1}{N_k - 1} \sum_{j \in B_k \setminus \{i\}} \langle z_i, z_j \rangle \right)} \right) \\ &= \log \left(\frac{\sum_{l \in B_k \setminus \{i\}} \exp\left(\langle z_i, z_l \rangle \right) + \sum_{\substack{k' \in [K] \\ k' \neq k}} \sum_{m \in B_{k'}} \exp\left(\langle z_i, z_m \rangle \right)}{\exp\left(\frac{1}{N_k - 1} \sum_{j \in B_k \setminus \{i\}} \langle z_i, z_j \rangle \right)} \right). \end{aligned} \tag{34}$$

There are three terms in Eq. (34). Let's check their lower bounds one by one. Applying Jensen's inequity, the first term can be bounded below:

$$\sum_{l \in B_k \setminus \{i\}} \exp\left(\langle z_i, z_l \rangle \right) \geq (N_k - 1) \exp\left(\frac{1}{(N_k - 1)} \sum_{l \in B_k \setminus \{i\}} \langle z_i, z_l \rangle \right), \tag{35}$$

where equality is attained if and only if all of the following conditions hold:

(C1) $\forall k \in [K]$ and $\forall i \in B_k$, $\exists \alpha(k, i)$ such that $\forall j \in B_k \setminus \{i\}$, all inner products $\langle z_i, z_j \rangle = \alpha(k, i)$ are equal.

Let $\bar{z}_k = \frac{1}{N_k} \sum_{i \in B_k} z_i$. Similarly, the second term can be bounded below:

$$\begin{aligned} \sum_{m \in B_{k'}} \exp\left(\langle z_i, z_m \rangle \right) &\geq N_{k'} \exp\left(\frac{1}{N_{k'}} \sum_{m \in B_{k'}} \langle z_i, z_m \rangle \right) = N_{k'} \exp\left(\left\langle z_i, \frac{1}{N_{k'}} \sum_{m \in B_{k'}} z_m \right\rangle \right), \\ &= N_{k'} \exp\left(\langle z_i, \bar{z}_{k'} \rangle \right) \end{aligned} \tag{36}$$

where equality is attained if and only if all of the following conditions hold:

(C2) $\forall k \in [K]$ and $\forall i \in B_k$, $\exists \alpha(k, i, k')$ such that $k' \in [K] \setminus \{k\}$ and $m \in B_{k'}$, all inner products $\langle z_i, z_m \rangle = \alpha'(k, i, k')$ are equal. And $\alpha'(k, i, k') = \langle z_i, \bar{z}_{k'} \rangle$.

Using Cauchy-Schwarz inequality, the third term can be bounded below:

$$\frac{1}{\exp\left(\frac{1}{N_k - 1} \sum_{j \in B_k \setminus \{i\}} \langle z_i, z_j \rangle \right)} \geq \frac{1}{\exp\left(\frac{1}{N_k - 1} \sum_{j \in B_k \setminus \{i\}} \|z_i\| \, \|z_j\| \right)} = e^{-1}, \tag{37}$$

where equality is attained if and only if the following condition holds:

(C3) $\forall k \in [K]$ and $\forall i, j \in B_k$, $z_i = z_j = \bar{z}_k$.

It's obvious to see that when condition (C3) holds, all samples from the same class collapse into their class center (denoted by $\bar{z}_k$). In this case, and thus condition (C1) and (C2) hold as well where

$\alpha(k,i)=1$ and $\alpha'(k,i,k')=\langle z_k,\bar{z}_{k'}\rangle$. So (C3) is a sufficient condition for (C1) and (C2). Now we have:

$$
\begin{aligned}
\sum_{i\in B_k}\mathcal{L}_{\mathrm{SC}}^{k,i} &= \sum_{i\in B_k}\log\left(\frac{\sum_{k\in B_k\setminus\{i\}}\exp\left(\langle z_i,z_l\rangle\right)+\sum_{\substack{k'\in[K]\\k'\neq k}}\sum_{l\in B_{k'}}\exp\left(\langle z_i,z_l\rangle\right)}{\exp\left(\frac{1}{N_k-1}\sum_{j\in B_k\setminus\{i\}}\langle z_i,z_j\rangle\right)}\right)\\
&\overset{Eq.\ (35)}{\geq} \sum_{i\in B_k}\log\left(\frac{(N_k-1)\exp\left(\frac{1}{(N_k-1)}\sum_{l\in B_k\setminus\{i\}}\langle z_i,z_l\rangle\right)+\sum_{\substack{k'\in[K]\\k'\neq k}}\sum_{l\in B_{k'}}\exp\left(\langle z_i,z_l\rangle\right)}{\exp\left(\frac{1}{N_k-1}\sum_{j\in B_k\setminus\{i\}}\langle z_i,z_j\rangle\right)}\right)\\
&= \sum_{i\in B_k}\log\left((N_k-1)+\frac{\sum_{\substack{k'\in[K]\\k'\neq k}}\sum_{l\in B_{k'}}\exp\left(\langle z_i,z_l\rangle\right)}{\exp\left(\frac{1}{N_k-1}\sum_{j\in B_k\setminus\{i\}}\langle z_i,z_j\rangle\right)}\right)\\
&\overset{Eq.\ (36)}{\geq} \sum_{i\in B_k}\log\left((N_k-1)+\frac{\sum_{\substack{k'\in[K]\\k'\neq k}}N_{k'}\exp\left(\langle z_i,\bar{z}_{k'}\rangle\right)}{\exp\left(\frac{1}{N_k-1}\sum_{j\in B_k\setminus\{i\}}\langle z_i,z_j\rangle\right)}\right)\\
&\overset{Eq.\ (37)}{\geq} \sum_{i\in B_k}\log\left((N_k-1)+e^{-1}\sum_{\substack{k'\in[K]\\k'\neq k}}N_{k'}\exp\left(\langle\bar{z}_k,\bar{z}_{k'}\rangle\right)\right)\\
&= N_k\log\left((N_k-1)+e^{-1}\sum_{\substack{k'\in[K]\\k'\neq k}}N_{k'}\exp\left(\langle\bar{z}_k,\bar{z}_{k'}\rangle\right)\right),
\end{aligned}
\tag{38}
$$

where equality is attained if and only if the following condition holds:

(B1) $\forall i\in B_k,\ z_i=\bar{z}_k$.

Here (B1) and (C3) express the same condition. □

Lemma 3. *Let $\bar{Z}$ be an K point configuration (assuming all $\bar{z}$s being normalized), $\bar{Z}=(\bar{z}_1,\ldots,\bar{z}_K)\in(\mathbb{S}^{h-1})^K$, and $K\leq h+1$, it holds that:*

$$
\sum_{k=1}^{K}a\log\left((a-1)+b\left(\sum_{\substack{k'\in[K]\\k'\neq k}}\exp\left(\langle\bar{z}_k,\bar{z}_{k'}\rangle\right)+c\right)\right)\geq Ka\log\left((a-1)+b\left((K-1)\exp\left(\beta\right)+c\right)\right),
\tag{39}
$$

where $a>1$, $b,c>0$, and equality is attained if and only if all of the following conditions hold:

(B2) $\forall k\in[K]$ and $k'\in[K]\setminus\{k\}$, $\langle\bar{z}_k,\bar{z}_{k'}\rangle=\beta$.

(B3) There exists a configuration of $\bar{Z}=(\bar{z}_1,\ldots,\bar{z}_K)$ such that (B2) holds.

(Case 1) $K=h+1$: $\beta=-\frac{1}{N-1}$ or $\beta=1$

(Case 2) $K<h+1$: $-\frac{1}{N-1}\leq\beta\leq 1$

Proof. Since $f(x) = \exp(x)$ is a convex function, applying Jensen's inequality, we have

$$\begin{aligned}\sum_{\substack{k' \in [K] \\ k' \neq k}} \exp\left(\langle \bar{z}_k, \bar{z}_{k'} \rangle\right) &\geq (K-1) \exp\left(\frac{1}{K-1} \sum_{\substack{k' \in [K] \\ k' \neq k}} \langle \bar{z}_k, \bar{z}_{k'} \rangle\right) \\ &= (K-1) \exp\left(\frac{1}{K-1} \sum_{\substack{k' \in [K] \\ k' \neq k}} \beta_k\right) \\ &= (K-1) \exp\left(\beta_k\right),\end{aligned} \tag{40}$$

where equality is attained if and only if all of the following conditions hold:

(C4) $\forall k \in [K]$ and $k' \in [K] \backslash \{k\}$, $\langle \bar{z}_k, \bar{z}_{k'} \rangle = \beta_k$.

(C5) There exists a configuration of $\bar{Z} = (\bar{z}_1, \ldots, \bar{z}_K)$ such that (C4) holds.

When $a > 1, b, c > 0$, $f(x) = \log\left((a-1) + b\left(\exp\left(x\right) + c\right)\right)$ is also a convex function. By Jensen's inequality, we have

$$\begin{aligned}\sum_{k=1}^{K} a \log\left((a-1) + b\left(\exp\left(\beta_k\right) + c\right)\right) &\geq Ka \log\left((a-1) + b\left(\exp\left(\frac{1}{K}\sum_{k=1}^{K} \beta_k\right) + c\right)\right) \\ &= Ka \log\left((a-1) + b\left(\exp\left(\frac{1}{K}\sum_{k=1}^{K} \beta\right) + c\right)\right) \\ &= Ka \log\left((a-1) + b\left(\exp\left(\beta\right) + c\right)\right),\end{aligned} \tag{41}$$

where equality is attained if and only if all of the following conditions hold:

(C6) $\forall k \in [K]$ and $k' \in [K] \backslash \{k\}$, $\beta_k = \beta_{k'} = \beta$.

(C7) There exists a configuration of $\bar{Z} = (\bar{z}_1, \ldots, \bar{z}_K)$ such that (C6) holds.

Note that when (C6) and (C7) hold, (C4) and (C5) hold too. And according to Lemma 1, when $K \leq h + 1$, Case 2 and Case 3 in Lemma 1 satisfy (C7). And hence

$$\sum_{k=1}^{K} a \log\left((a-1) + b\left(\sum_{\substack{k' \in [K] \\ k' \neq k}} \exp\left(\langle \bar{z}_k, \bar{z}_{k'} \rangle\right) + c\right)\right) \geq Ka \log\left((a-1) + b\left((K-1)\exp\left(\beta\right) + c\right)\right), \tag{42}$$

where equality is attained if and only if all of the following conditions hold:

(B2) $\forall k \in [K]$ and $k' \in [K] \backslash \{k\}$, $\langle \bar{z}_k, \bar{z}_{k'} \rangle = \beta$.

(B3) There exists a configuration of $\bar{Z} = (\bar{z}_1, \ldots, \bar{z}_K)$ such that (B2) holds

(Case 1) $K = h + 1$: $\beta = -\frac{1}{N-1}$ or $\beta = 1$

(Case 2) $K < h + 1$: $-\frac{1}{N-1} \leq \beta \leq 1$

□

B.2 PROOF OF THEOREM 2

In this section, we provide proofs for Theorem 2 proposed in Sec. 3.2. For the convenience of your reading, let's recall some related notions and definitions.

- $h, N, K \in \mathbb{N}$
- $\mathcal{Z} = \mathbb{R}^h$
- $\mathbb{S}^{h-1} = \left\{z \in \mathbb{R}^h : \|z\| = 1\right\}$
- $\mathcal{Y} = \{1, \ldots, K\} = [K]$
- $B = \{1, \ldots, N\} = [N]$
- $B_k = \{i : i \in B, y_i = k\}$
- $N_k = |B_k|$

Definition 1 (Supervised contrastive loss) Let Z be an N point configuration (assuming all zs being normalized), $Z = (z_1, \ldots, z_N) \in (\mathbb{S}^{h-1})^N$, with labels $Y = (y_1, \ldots, y_N) \in ([K])^N$, and $K \leq h + 1$. Let $B = [N]$, $B_k = \{i : i \in B, y_i = k\}$ and $N_k = |B_k|$. The supervised contrastive loss $\mathcal{L}_{\mathrm{SC}}(\cdot; Y) : (\mathbb{S}^{h-1})^N \to \mathbb{R}$ is defined as:

$$\mathcal{L}_{\mathrm{SC}} = \sum_{k=1}^{K} \sum_{i \in B_k} \mathcal{L}_{\mathrm{SC}}^{k,i}, \text{ where } \mathcal{L}_{\mathrm{SC}}^{i} = -\frac{\mathbb{1}_{\{N_k > 1\}}}{N_k - 1} \sum_{j \in B_k \setminus \{i\}} \log \left(\frac{\exp\left(\langle z_i, z_j \rangle\right)}{\sum_{l \in B \setminus \{i\}} \exp\left(\langle z_i, z_l \rangle\right)} \right).$$

Theorem 2 Let Z be an N point configuration (assuming all zs being normalized), $Z = (z_1, \ldots, z_N) \in (\mathbb{S}^{h-1})^N$, with labels $Y = (y_1, \ldots, y_N) \in ([K])^N$, and $3 \leq K \leq h + 1$. If $\forall k \in \{2, \ldots, K\}, N_k = a_2 \geq 4$, and $\exists \rho > 0$ such that $N_1 = a_1 = \rho a_2 > 1$, it holds that:

$$\mathcal{L}_{\mathrm{SC}} \geq f(\cos(\theta_1), \cos(\theta_2)),$$

where $f(\cdot) : \mathbb{R} \times \mathbb{R} \to \mathbb{R}$ is defined as:

$$\begin{aligned} f(x_1, x_2) = {} & \rho a_2 \log\left(\left(\rho a_2 - 1\right) + e^{-1}\left(K - 1\right) a_2 \exp\left(x_1\right)\right) \\ & + (K-1) a_2 \log\left(\left(a_2 - 1\right) + e^{-1}\left(\left(K - 2\right) a_2 \exp\left(x_2\right) + \rho a_2 \exp\left(x_1\right)\right)\right), \end{aligned}$$

and equality is attained if and only if there exists a configuration of $\bar{Z} = (\bar{z}_1, \ldots, \bar{z}_K) \in (\mathbb{S}^{h-1})^K$ such that:

(A3) $i \in B_k$, $z_i = \bar{z}_k$.

(A4) $\forall k, k' \in \{2, \ldots, K\}$ and $k \neq k'$, $\langle \bar{z}_1, \bar{z}_k \rangle = \cos(\theta_1)$, $\langle \bar{z}_k, \bar{z}_{k'} \rangle = \cos(\theta_2), and \cos(\theta_2) = \frac{(K-1)\cos^2(\theta_1) - 1}{K-2}$.

(A5) (Case 1) $\rho < 1$: $\theta_1 \in \left(\cos^{-1}(-\frac{1}{K-1}), 0\right)$ such that $f'_{x_1}(\cos(\theta_1)) = 0$.

(Case 2) $\rho = 1$: $\theta_1 = \cos^{-1}(-\frac{1}{K-1})$.

(Case 3) $1 < \rho < R(K, a_2)$: $\theta_1 \in \left(-\pi, \cos^{-1}(-\frac{1}{K-1})\right)$ such that $f'_{x_1}(\cos(\theta_1)) = 0$.

(Case 4) $\rho \geq R(K, a_2)$: $\theta_1 = -\pi$.

Let $b_1 = (K-1)(1+e^{-2}-2e^2)a_2 - 2$, $b_2 = 8(1+e^{-2})(K-1)a_2((K-1)a_2 - e^2)$, then $R(K, a_2)$ defined as:

$$R(K, a_2) = \frac{-b_1 + \sqrt{b_1^2 + b_2}}{2(1 + e^{-2})a_2}.$$

B.2.1 STEPS OF PROOF

Following Eq. (27), Eq. (28) and Lemma 2 in Appendix B.1.1, we have

$$\mathcal{L}_{\mathrm{SC}} \overset{Lemma\ 2}{\geq} \sum_{k=1}^{K} N_k \log \left((N_k - 1) + e^{-1} \sum_{\substack{k' \in [K] \\ k' \neq k}} N_{k'} \exp\left(\langle \bar{z}_k, \bar{z}_{k'} \rangle\right) \right). \tag{43}$$

where equality is attained if and only if there exists a configuration of $\bar{Z} = (\bar{z}_1, \ldots, \bar{z}_K) \in (\mathbb{S}^{h-1})^K$ such that:

(A3) $i \in B_k$, $z_i = \bar{z}_k$.

When $3 \leq K \leq h+1$, $\forall k \in \{2, \ldots, K\}$, $N_k = a_2 \geq 4$, and $\exists \rho > 0$ such that $N_1 = a_1 = \rho a_2 > 1$, following Lemma 5, we have:

$$\begin{aligned} \mathcal{L}_{\mathrm{SC}} &\geq \sum_{k=1}^{K} N_k \log \left((N_k - 1) + e^{-1} \sum_{\substack{k' \in [K] \\ k' \neq k}} N_{k'} \exp\left(\langle \bar{z}_k, \bar{z}_{k'} \rangle\right) \right) \\ &\overset{Lemma\ 5}{\geq} f(\beta_1), \end{aligned} \tag{44}$$

where $f(x)$ is:

$$\begin{aligned} f(x) = {} & \rho a_2 \log\left((\rho a_2 - 1) + e^{-1} (K-1) a_2 \exp(x) \right) \\ & + (K-1) a_2 \log\left((a_2 - 1) + e^{-1} \left((K-2) a_2 \exp\left(\frac{(K-1)x^2 - 1}{K-2} \right) + \rho a_2 \exp(x) \right) \right), \end{aligned} \tag{45}$$

and equality is attained if and only if all of the following conditions hold:

(A4) $\forall k, k' \in \{2, \ldots, K\}$ and $k \neq k'$, $\langle \bar{z}_1, \bar{z}_k \rangle = \cos(\theta_1)$, $\langle \bar{z}_k, \bar{z}_{k'} \rangle = \cos(\theta_2)$, *and* $\cos(\theta_2) = \frac{(K-1)\cos^2(\theta_1) - 1}{K-2}$.

(A5) (Case 1) $\rho < 1$: $\theta_1 \in \left(\cos^{-1}(-\frac{1}{K-1}), 0 \right)$ such that $f'_{x_1}(\cos(\theta_1)) = 0$.

(Case 2) $\rho = 1$: $\theta_1 = \cos^{-1}(-\frac{1}{K-1})$.

(Case 3) $1 < \rho < R(K, a_2)$: $\theta_1 \in \left(-\pi, \cos^{-1}(-\frac{1}{K-1}) \right)$ such that $f'_{x_1}(\cos(\theta_1)) = 0$.

(Case 4) $\rho \geq R(K, a_2)$: $\theta_1 = -\pi$.

Here $b_1 = (K-1)(1 + e^{-2} - 2e^2)a_2 - 2$ and $b_2 = 8(1 + e^{-2})(K-1)a_2((K-1)a_2 - e^2)$. $R(K, a_2)$ is given by:

$$R(K, a_2) = \frac{-b_1 + \sqrt{b_1^2 + b_2}}{2(1 + e^{-2})a_2}. \tag{46}$$

B.2.2 LEMMAS PART 2

In this section,we provide definitions and proofs of lemmas that are used for the proof of Theorem 2.

Lemma 4. *Let $\bar{Z}$ be an K point configuration (assuming all $\bar{z}$s being normalized), $\bar{Z} = (\bar{z}_1, \ldots, \bar{z}_K) \in (\mathbb{S}^{h-1})^K$, and $3 \leq K \leq h+1$. If $\forall k, k' \in \{2, \ldots, K\}$ and $k \neq k'$ such that $\langle \bar{z}_k, \bar{z}_{k'} \rangle = \beta_2$ and $\beta_1 = min_c\{c : \langle \bar{z}_1, \bar{z}_k \rangle = c\}$, it holds that:*

$$\beta_2 = \frac{(K-1)\beta_1^2 - 1}{K-2}, \text{ where } -1 \leq \beta_1 \leq 0 \text{ and } -\frac{1}{K-2} \leq \beta_2 < 1. \tag{47}$$

Proof. Without loss of generality, we assume $(\bar{z}_2, \ldots, \bar{z}_K)$ form an equidistant simplex in the southern hemisphere of $\mathbb{S}^{h-1}$ and then $\bar{z}_1$ is at the north pole. Let $l = \|\frac{1}{K-1}\sum_{k=2}^{K} z_k\|$, we have $l = |\beta_1|$, then

$$\begin{aligned}
\|l\|^2 &= \left\| \frac{1}{K-1} \sum_{k=2}^{K} z_k \right\|^2 = \left\langle \frac{1}{K-1} \sum_{k=2}^{K} z_k, \frac{1}{K-1} \sum_{k=2}^{K} z_k \right\rangle \\
&= \frac{1}{(K-1)^2} \left(\sum_{k=2}^{K} z_k \langle z_k, z_k \rangle + \sum_{\substack{k,k'=2 \\ k \neq k'}}^{K} \langle z_k, z_{k'} \rangle \right) \\
&= \frac{1}{(K-1)^2} \left((K-1) + (K-1)(K-2)\beta_2 \right) \\
&= |\beta_1|^2,
\end{aligned} \tag{48}$$

so we have

$$\beta_2 = \frac{(K-1)\beta_1^2 - 1}{K-2}. \tag{49}$$

According to Lemma 1, $-\frac{1}{K-2} \leq \beta_2 < 1$ and so $-1 \leq \beta_1 \leq 0$. □

Lemma 5. *Let $\bar{Z}$ be an K point configuration (assuming all $\bar{z}s$ being normalized), $\bar{Z} = (\bar{z}_1, \ldots, \bar{z}_K) \in (\mathbb{S}^{h-1})^K$, and $3 \leq K \leq h+1$. Let $B = [N]$, $B_k = \{i : i \in B, y_i = k\}$ and $N_k = |B_k|$. Let $\mathcal{J}(\cdot) : (\mathbb{S}^{h-1})^K \to \mathbb{R}$ is defined as:*

$$\mathcal{J}(\bar{Z}) = \sum_{k=1}^{K} N_k \log \left((N_k - 1) + e^{-1} \sum_{\substack{k' \in [K] \\ k' \neq k}} N_{k'} \exp\left(\langle \bar{z}_k, \bar{z}_{k'} \rangle \right) \right), \tag{50}$$

If $\forall k \in \{2, \ldots, K\}, N_k = a_2 \geq 4$, and $\exists \rho > 0$ such that $N_1 = a_1 = \rho a_2 > 1$, it holds that:

$$\mathcal{J}(\bar{Z}) \geq f(\beta_1), \tag{51}$$

where $f(\cdot) : \mathbb{R} \to \mathbb{R}$ is defined as:

$$\begin{aligned}
f(x) &= \rho a_2 \log\left((\rho a_2 - 1) + e^{-1}(K-1) a_2 \exp(x) \right) \\
&\quad + (K-1) a_2 \log\left((a_2 - 1) + e^{-1} \left((K-2) a_2 \exp\left(\frac{(K-1)x^2 - 1}{K-2} \right) + \rho a_2 \exp(x) \right) \right),
\end{aligned} \tag{52}$$

and equality is attained if and only if all of the following conditions hold:

- *(B4)* $\forall k, k' \in \{2, \ldots, K\}$ *and* $k \neq k'$, $\langle \bar{z}_1, \bar{z}_k \rangle = \beta_1$ *and* $\langle \bar{z}_k, \bar{z}_{k'} \rangle = \beta_2 = \frac{(K-1)\beta_1^2 - 1}{K-2}$.
- *(B5) (Case 1)* $\rho < 1$*:* $\hat{x} \in (-\frac{1}{K-1}, 0)$.
  (Case 2) $\rho = 1$*:* $\hat{x} = -\frac{1}{K-1}$.
  (Case 3) $1 < \rho < R(K, a_2)$*:* $\hat{x} \in (-1, -\frac{1}{K-1})$.
  (Case 4) $\rho \geq R(K, a_2)$*:* $\hat{x} = -1$.

Here $b_1 = (K-1)(1+e^{-2}-2e^2)a_2 - 2$ and $b_2 = 8(1+e^{-2})(K-1)a_2((K-1)a_2 - e^2)$. $R(K, a_2)$ is given by:

$$R(K, a_2) = \frac{-b_1 + \sqrt{b_1^2 + b_2}}{2(1+e^{-2})a_2}. \tag{53}$$

Proof. When $N_1 = a_1, \forall k \in \{2, \ldots, K\}, N_k = a_2, a_1 = \rho a_2$, then

$$\begin{aligned}\mathcal{J}(\bar{Z}) &= \sum_{k=1}^{K} N_k \log \left((N_k - 1) + e^{-1} \sum_{\substack{k' \in [K] \\ k' \neq k}} N_{k'} \exp\left(\langle \bar{z}_k, \bar{z}_{k'} \rangle\right) \right) \\ &= a_1 \log \left((a_1 - 1) + e^{-1} \sum_{k'=2}^{K} a_2 \exp\left(\langle \bar{z}_1, \bar{z}_{k'} \rangle\right) \right) \\ &+ \sum_{k=2}^{K} a_2 \log \left((a_2 - 1) + e^{-1} \left(\sum_{\substack{k'=2 \\ k' \neq k}}^{K} a_2 \exp\left(\langle \bar{z}_k, \bar{z}_{k'} \rangle\right) + a_1 \exp\left(\langle \bar{z}_k, \bar{z}_1 \rangle\right) \right) \right).\end{aligned} \tag{54}$$

According to Eq. (40) in the Lemma 3, the first term can be bounded low:

$$\begin{aligned}&a_1 \log \left((a_1 - 1) + e^{-1} \sum_{k'=2}^{K} a_2 \exp\left(\langle \bar{z}_1, \bar{z}_{k'} \rangle\right) \right) \\ &\geq a_1 \log \left((a_1 - 1) + e^{-1} (K-1) a_2 \exp(\beta_1) \right) \\ &= f_1(\beta_1).\end{aligned} \tag{55}$$

Similarly, the second term can be bounded low:

$$\begin{aligned}&\sum_{k=2}^{K} a_2 \log \left((a_2 - 1) + e^{-1} \left(\sum_{\substack{k'=2 \\ k' \neq k}}^{K} a_2 \exp\left(\langle \bar{z}_k, \bar{z}_{k'} \rangle\right) + a_1 \exp\left(\langle \bar{z}_k, \bar{z}_1 \rangle\right) \right) \right) \\ &\geq (K-1) a_2 \log \left((a_2 - 1) + e^{-1} \left((K-2) a_2 \exp(\beta_2) + a_1 \exp(\beta_1) \right) \right) \\ &= f_2(\beta_1).\end{aligned} \tag{56}$$

Combining Eq. (55), Eq. (56) and Lemma 4, we have

$$\begin{aligned}\mathcal{J}(\bar{Z}) &\geq \rho a_2 \log \left((\rho a_2 - 1) + e^{-1} (K-1) a_2 \exp(\beta_1) \right) \\ &+ (K-1) a_2 \log \left((a_2 - 1) + e^{-1} \left((K-2) a_2 \exp\left(\frac{(K-1)\beta_1^2 - 1}{K-2} \right) + \rho a_2 \exp(\beta_1) \right) \right) \\ &= f_1(\beta_1) + f_2(\beta_1) = f(\beta_1),\end{aligned} \tag{57}$$

where $-1 \leq \beta_1 \leq 0$ and equality is attained if and only if the following condition holds:

(C8) $\forall k, k' \in \{2, \ldots, K\}$ and $k \neq k'$, $\langle \bar{z}_1, \bar{z}_k \rangle = \beta_1$ and $\langle \bar{z}_k, \bar{z}_{k'} \rangle = \beta_2 = \frac{(K-1)\beta_1^2 - 1}{K-2}$.

To find the minimal value of $f(x)$ when $-1 \leq x \leq 0$, we need to find the critical value of $f'(x) = 0$ and the sign of $f'(x)$. Direct computation of these value is difficult but can be found with scientific computation software once we know all parameters in a specific case. For analytical purpose, we investigate the general form. Let $3 \leq K \leq h + 1, \rho > 0, a_1 = \rho a_2 > 1, a_2 \geq 4$ and $-1 \leq x \leq 0$.

We first study key properties of $f(x)$.

(P1) We start by analyzing the derivatives of $f(x)$. The first and the second derivative of $f_1(x)$ are:

$$f_1'(x) = e^{-1}(K-1)a_2^2 \frac{\rho e^x}{(\rho a_2 - 1) + e^{-1}(K-1)a_2 e^x} > 0, \tag{58}$$

and

$$f_1''(x) = e^{-1}(K-1)a_2^2 \frac{(\rho a_2 - 1)\, \rho e^x}{((\rho a_2 - 1) + e^{-1}(K-1)a_2 e^x)^2} > 0. \tag{59}$$

Here $f_1'(x)$ and $f_1''(x)$ are strictly positive because every term of them is positive. The First derivative of $f_2(x)$ is:

$$f_2'(x) = e^{-1}(K-1)a_2^2 \frac{2(K-1)x\exp\left(\frac{(K-1)x^2-1}{K-2}\right) + \rho e^x}{(a_2-1) + e^{-1}\left((K-2)a_2\exp\left(\frac{(K-1)x^2-1}{K-2}\right) + \rho a_2 e^x\right)}. \tag{60}$$

The second derivative of $f_2(x)$ is difficult to calculate directly. We instead do it in another way. If we take $y(x) = \exp(\frac{(K-1)x^2-1}{K-2})$ as a variable, we have:

$$\frac{dy(x)}{dx} = \frac{2(K-1)x}{K-2}\exp(\frac{(K-1)x^2-1}{K-2}) < 0. \tag{61}$$

It holds because every term but x (negative) in $\frac{dy(x)}{dx}$ is positive. And $f_2'(x)$ can be written as:

$$\begin{aligned} f_2'(x) = G(x,y) &= e^{-1}(K-1)a_2^2 \frac{\rho e^x + 2(K-1)xy}{(a_2-1) + e^{-1}\rho a_2 e^x + e^{-1}(K-2)a_2 y} \\ &= c_1\frac{c_2 + c_3 y}{c_4 + c_5 y}, \end{aligned} \tag{62}$$

where $c_1 = e^{-1}(K-1)a_2^2 > 0$, $c_2 = \rho e^x$, $c_3 = 2(K-1)x$, $c_4 = (a_2-1) + e^{-1}\rho a_2 e^x$, $c_5 = e^{-1}(K-2)a_2$ and $-1 \le x \le 0$. Then the partial derivative of G to y is:

$$\begin{aligned} \frac{\partial G(x,y)}{\partial y} &= \frac{c_1}{(c_4 + c_5 y)^2}\left(c_3 c_4 - c_2 c_5\right) \\ &= \frac{c_1}{(c_4 + c_5 y)^2}\left(\left(2(K-1)x - (K-2)\right)e^{-1}\rho a_2 e^x + (a_2-1)2(K-1)x\right) \\ &< 0. \end{aligned} \tag{63}$$

Here $\frac{\partial G}{\partial y}$ is strictly negative because $(2(K-1)x - (K-2))$ and x are negative while all other terms are positive. Similarly, $f_2'(x)$ can be written as:

$$\begin{aligned} f_2'(x) = G(x,y) &= e^{-1}(K-1)a_2^2 \frac{2(K-1)yx + \rho e^x}{(a_2-1) + e^{-1}(K-2)a_2 y + e^{-1}\rho a_2 e^x} \\ &= c_1\frac{c_6 x + c_7 e^x}{c_8 + c_9 e^x}, \end{aligned} \tag{64}$$

where $c_1 = e^{-1}(K-1)a_2^2$, $c_6 = 2(K-1)y$, $c_7 = \rho$, $c_8 = (a_2-1) + e^{-1}(K-2)a_2 y$, $c_9 = e^{-1}\rho a_2$ and $-1 \le x \le 0$. Here $c_1, c_6, c_7, c_8, c_9 > 0$. Then the partial derivative of G to x is:

$$\frac{\partial G(x,y)}{\partial x} = \frac{c_1}{(c_8 + c_9 e^x)^2}\left((1-x)c_6 c_9 e^x + c_7 c_8 e^x + c_6 c_8\right) > 0. \tag{65}$$

Here $\frac{\partial G}{\partial x}$ is strictly positive because every term of it is positive. Combining Eq. (61), Eq. (63) and Eq. (65), we have:

$$f_2''(x) = \frac{\partial G(x,y)}{\partial x} + \frac{\partial G(x,y)}{\partial y}\cdot\frac{dy(x)}{x} > 0. \tag{66}$$

Thus, according to Eq. (59) and Eq. (66), the second derivative of $f(x)$ is:

$$f''(x) = f_1''(x) + f_2''(x) > 0. \tag{67}$$

This reveals that $f(x)$ is a convex function.

(P2) Next, we analyze how ρ affects $f'(x)$. If we view ρ as a variable instead of a constant, we have

$$\begin{aligned} f_1'(x) = H_1(x,\rho) &= e^{-1}(K-1)a_2^2 e^x \frac{\rho}{a_2\rho + e^{-1}(K-1)a_2 e^x - 1} \\ &= c_1\frac{\rho}{a_2\rho + c_2}, \end{aligned} \tag{68}$$

where $c_1 = e^{-1}(K-1)a_2^2 e^x$ ¿ 0, $c_2 = e^{-1}(K-1)a_2 e^x - 1$. Then the partial derivative of H_1 to ρ is given by:

$$\begin{aligned}\frac{\partial H_1(x,\rho)}{\partial \rho} &= c_1 \frac{c_2}{(a_2\rho + c_2)^2} = c_1 \frac{e^{-1}(K-1)a_2 e^x - 1}{(a_2\rho + c_2)^2} \\ &> c_1 \frac{e^{-1}(3-1)a_2 e^{-1} - 1}{(a_2\rho + c_2)^2} = c_1 \frac{2e^{-2}a_2 - 1}{(a_2\rho + c_2)^2} \\ &> 0.\end{aligned} \tag{69}$$

When $K \geq 3$ and $-1 \leq x \leq 0$, $e^{-1}(K-1)a_2 e^x > 2e^{-2}a_2$. So as long as $a_2 \geq 4 > \frac{e^2}{2}$ holds, $c_2 > 0$ holds. Similarly, we also have:

$$\begin{aligned}f_2'(x) = H_2(x,\rho) &= e^{-1}(K-1)a_2^2 e^x \frac{\rho + 2(K-1)xe^{-x}\exp\left(\frac{(K-1)x^2-1}{K-2}\right)}{e^{-1}a_2 e^x \rho + (a_2-1) + e^{-1}(K-2)a_2 \exp\left(\frac{(K-1)x^2-1}{K-2}\right)} \\ &= c_1 \frac{\rho + c_3}{c_4\rho + c_5},\end{aligned} \tag{70}$$

where $c_1 = e^{-1}(K-1)a_2^2 e^x$ ¿ 0, $c_3 = 2(K-1)xe^{-x}\exp\left(\frac{(K-1)x^2-1}{K-2}\right)$, $c_4 = e^{-1}a_2 e^x$ and $c_5 = (a_2-1) + e^{-1}(K-2)a_2\exp\left(\frac{(K-1)x^2-1}{K-2}\right)$. Then the partial derivative of H_2 to ρ is:

$$\begin{aligned}\frac{\partial H_2(x,\rho)}{\partial \rho} &= c_1 \frac{c_5 - c_3 c_4}{(c_4\rho + c_5)^2} = c_1 \frac{(a_2-1) + e^{-1}a_2(-Kx)\exp\left(\frac{(K-1)x^2-1}{K-2}\right)}{(c_4\rho + c_5)^2} \\ &> 0.\end{aligned} \tag{71}$$

It holds because every term in $\frac{\partial H_2}{\partial \rho}$ is positive. Combining Eq. (68) to Eq. (71), we have

$$\begin{aligned}f'(x) &= f_1'(x) + f_2'(x) \\ &= H_1(x,\rho) + H_2(x,\rho) = H(x,\rho),\end{aligned} \tag{72}$$

and

$$\frac{\partial H(x,\rho)}{\partial \rho} = \frac{\partial H_1(x,\rho)}{\partial \rho} + \frac{\partial H_2(x,\rho)}{\partial \rho} > 0. \tag{73}$$

So $f'(x) = H(x,\rho)$ is an increasing function with respect to ρ.

With the above 2 key properties of $f(x)$ in hand. Now, let's check some important values.

(V1). When $x = 0$, we have:

$$\begin{aligned}f'(0) &= \frac{e^{-1}(K-1)\rho a_2^2}{(\rho a_2 - 1) + e^{-1}(K-1)a_2} + \frac{e^{-1}(K-1)\rho a_2^2}{(a_2-1) + e^{-1}\left((K-2)a_2\exp\left(-\frac{1}{K-2}\right) + \rho a_2\right)} \\ &> 0.\end{aligned} \tag{74}$$

It holds because every term in $f'(0)$ is positive. This case shows that, when samples from $K-1$ equal-sized classes are well-trained, they form a $K-2$ regular simplex ($\beta_1 = 0$ and $\beta_2 = -\frac{1}{K-2}$). Once there comes samples from the K^{th} class, the original $K-2$ simplex starts to shrink as the loss goes down when β_1 decreases and β_2 increases.

(V2). When $x = -\frac{1}{K-1}$, we have:

$$\begin{aligned}f'(-\frac{1}{K-1}) &= H(-\frac{1}{K-1}, \rho) \\ &= \frac{e^{-1}(K-1)a_2^2 e^{-\frac{1}{K-1}}\rho}{(\rho a_2 - 1) + e^{-1}(K-1)a_2 e^{-\frac{1}{K-1}}} + \frac{e^{-1}(K-1)a_2^2 e^{-\frac{1}{K-1}}(\rho - 2)}{(a_2-1) + e^{-1}a_2 e^{-\frac{1}{K-1}}((K-2+\rho)},\end{aligned} \tag{75}$$

and

$$H(-\frac{1}{K-1}, 1) = 0. \tag{76}$$

According to Eq. (72) and Eq. (73), $H(-\frac{1}{K-1}, \rho)$ is an increasing function with respect to ρ. Recalling that $f(x)$ is a convex function, with Eq. (75) and Eq. (76), we can conclude that:

(C9) When $\rho < 1$: $f'(-\frac{1}{K-1}) < H(-\frac{1}{K-1}, 1) = 0$. Since $f'(0) > 0$, according to the intermediate value theorem, there exists a critical point $\hat{x} \in (-\frac{1}{K-1}, 0)$, such that $f'(\hat{x}) = 0$, and $f(x)$ attains its minimal value at $x = \hat{x}$. If ρ increases, $f'(\hat{x})$ increases too. It leads to $f'(\hat{x}) > 0$, then there comes a new critical point $\tilde{x} \in (-\frac{1}{K-1}, \hat{x})$ where $f'(\tilde{x}) = 0$.

(C10) When $\rho = 1$: $f'(-\frac{1}{K-1}) = H(-\frac{1}{K-1}, 1) = 0$. So $\hat{x} = -\frac{1}{K-1}$ is the critical point and $f(x)$ attains its minimal value at $x = -\frac{1}{K-1}$.

(C11) When $\rho > 1$: $f'(-\frac{1}{K-1}) > H(-\frac{1}{K-1}, 1) = 0$. And $\forall x \in [-\frac{1}{K-1}, 0]$, $f'(x) > 0$ and $f(x) \geq f(-\frac{1}{K-1})$.

(V3). When $x = -1$, from (C7) and (C8) we know that $f'(-1) < 0$ if $\rho \leq 1$. Now let's only consider the case when $\rho > 1$.

$$\begin{aligned} f'(-1) &= \frac{e^{-2}(K-1)a_2^2\rho}{(\rho a_2 - 1) + e^{-2}(K-1)a_2} + (K-1)a_2^2 \frac{-2(K-1) + e^{-2}\rho}{(a_2 - 1) + (K-2)\, a_2 + e^{-2}\rho a_2} \\ &= e^{-2}(K-1)a_2^2 \left(\frac{\rho}{a_2\rho + e^{-2}(K-1)a_2 - 1} + \frac{\rho - 2(K-1)e^2}{e^{-2}a_2\rho + (K-1)\, a_2 - 1} \right) \\ &= e^{-2}(K-1)a_2^2 \left(\frac{\rho}{a_2\rho + c_1} + \frac{\rho + c_2}{e^{-2}a_2\rho + c_3} \right) \\ &= \frac{e^{-2}(K-1)a_2^2}{(a_2\rho + c_1)(e^{-2}a_2\rho + c_3)} \left((1 + e^{-2})a_2\rho^2 + (c_1 + c_3 + a_2c_2)\rho + c_1c_2 \right) \\ &= \frac{(K-1)e^{-2}a_2^2}{(a_2\rho + c_1)(e^{-2}a_2\rho + c_3)} \cdot L(\rho), \end{aligned} \tag{77}$$

where $c_1 = e^{-2}(K-1)a_2 - 1$, $c_2 = -2(K-1)e^2$, $c_3 = (K-1)\, a_2 - 1$ and:

$$\begin{aligned} L(\rho) &= (1 + e^{-2})a_2\rho^2 + (c_1 + c_3 + a_2c_2)\rho + c_1c_2 \\ &= (1 + e^{-2})a_2\rho^2 + ((K-1)(1 + e^{-2} - 2e^2)a_2 - 2)\rho - 2(K-1)((K-1)a_2 - e^2). \end{aligned} \tag{78}$$

When $K \geq 3$, as long as $a_2 \geq 4 > \frac{e^2}{2}$ holds, $c_1 > 2e^{-2}a_2 - 1 > 0$. Also $c_3 > 0$, so we have $\frac{(K-1)e^{-2}a_2^2}{(a_2\rho + c_1)(e^{-2}a_2\rho + c_3)} > 0$, then $f'(-1) \geq 0 \Leftrightarrow L(\rho) \geq 0$. To solve this inequality, let's first take a look the value:

$$\begin{aligned} M &= (c_1 + c_3 + a_2c_2)^2 - 4(1 + e^{-2})a_2c_1c_2 \\ &> -4(1 + e^{-2})a_2c_1c_2 \\ &= 8(1 + e^{-2})a_2(K-1)e^2c_1 \\ &> c_1 > 0. \end{aligned} \tag{79}$$

Let $b_1 = c_1 + c_3 + a_2c_2 = (K-1)(1 + e^{-2} - 2e^2)a_2 - 2 < 0$, $b_2 = -4(1 + e^{-2})a_2c_1c_2 = 8(1 + e^{-2})(K-1)a_2((K-1)a_2 - e^2) > 0$ and $M = b_1^2 + b_2 > 0$. Then the solution for $L(\rho) > 0$ and also $f'(-1) > 0$ is:

$$\rho \leq \frac{-b_1 - \sqrt{b_1^2 + b_2}}{2(1 + e^{-2})a_2} \text{or } \rho \geq \frac{-b_1 + \sqrt{b_1^2 + b_2}}{2(1 + e^{-2})a_2}. \tag{80}$$

Since $b_2 > 0$, then $\sqrt{b_1^2 + b_2} > -b_1$ and so $-b_1 - \sqrt{b_1^2 + b_2}$ ¡ 0. As we only consider the case where $\rho > 1$. We retain the right part of Eq. (80).

Combined with (C11), now we can conclude that: when $K \geq 3$ and $a_2 \geq 4$, let

$$R(K, a_2) = \frac{-b_1 + \sqrt{b_1^2 + b_2}}{2(1 + e^{-2})a_2}, \tag{81}$$

where $b_1 = (K-1)(1+e^{-2}-2e^2)a_2 - 2 < 0$ and $b_2 = 8(1+e^{-2})(K-1)a_2((K-1)a_2 - e^2) > 0$

(C12) When $1 < \rho < R(K, a_2)$: $f'(-1) < 0$. Since $\forall x \in [-\frac{1}{K-1}, 0]$, $f'(x) > 0$, according to the intermediate value theorem, there exists a critical point $\hat{x} \in (-1, -\frac{1}{K-1})$, such that $f'(\hat{x}) = 0$ and $f(x)$ attains its minimal value when $x = \hat{x}$. If ρ increases, $f'(\hat{x})$ increases too. It leads to $f'(\hat{x}) > 0$, then there comes a new critical point $\tilde{x} \in (-1, \hat{x})$ where $f'(\tilde{x}) = 0$.

(C13) When $\rho \geq R(K, a_2)$: $f'(-1) \geq 0$. Then $\forall x \in [-1, 0]$, $f'(x) \geq 0$. $f(x)$ attains its minimal value when $x = -1$

Combining (C8) to (C13), we conclude that: $\mathcal{J}(\bar{Z})$ reach its minimal if and only if all of the following conditions hold:

(B4) $\forall k, k' \in \{2, \ldots, K\}$ and $k \neq k'$, $\langle \bar{z}_1, \bar{z}_k \rangle = \beta_1$ and $\langle \bar{z}_k, \bar{z}_{k'} \rangle = \beta_2 = \frac{(K-1)\beta_1^2 - 1}{K-2}$.

(B5) (Case 1) $\rho < 1$: $\hat{x} \in (-\frac{1}{K-1}, 0)$.
(Case 2) $\rho = 1$: $\hat{x} = -\frac{1}{K-1}$.
(Case 3) $1 < \rho < R(K, a_2)$: $\hat{x} \in (-1, -\frac{1}{K-1})$.
(Case 4) $\rho \geq R(K, a_2)$: $\hat{x} = -1$.

□

B.3 Proof of Remark 2

Proof. Recall that:

$$R(K, a_2) = \frac{-b_1 + \sqrt{b_1^2 + b_2}}{2(1 + e^{-2})a_2}. \tag{82}$$

where $b_1 = (K-1)(1 + e^{-2} - 2e^2)a_2 - 2$, $b_2 = 8(1 + e^{-2})(K-1)a_2((K-1)a_2 - e^2)$. b_1 and b_2 in Eq. (82) can be roughly simplified as

$$\begin{aligned} \frac{b_1}{a_2} &= (K-1)(1 + e^{-2} - 2e^2) - \frac{2}{a_2} \approx (K-1)(1 + e^{-2} - 2e^2) = (K-1)b_1' \\ \frac{b_2}{a_2^2} &= 8(1 + e^{-2})(K-1)((K-1) - \frac{e^2}{a_2}) \approx 8(1 + e^{-2})(K-1)^2 = (K-1)^2 b_2', \end{aligned} \tag{83}$$

where $b_1' = (1 + e^{-2} - 2e^2)$ and $b_2' = 8(1 + e^{-2})$. Then we can roughly simplifies $R(K, a_2)$ as a function only respect to K as:

$$\begin{aligned} R(K, a_2) = \frac{-b_1 + \sqrt{b_1^2 + b_2}}{2(1 + e^{-2})a_2} &= \frac{-\frac{b_1}{a_2} + \sqrt{(\frac{b_1}{a_2})^2 + \frac{b_2}{a_2^2}}}{2(1 + e^{-2})} \\ &\approx (K-1)\frac{-b_1' + \sqrt{{b_1'}^2 + b_2'}}{2(1 + e^{-2})} \\ &= (K-1)\frac{-(1 + e^{-2} - 2e^2) + \sqrt{(1 + e^{-2} - 2e^2)^2 + 8(1 + e^{-2})}}{2(1 + e^{-2})} \\ &= R'(K) \end{aligned} \tag{84}$$

□